Systematic investigation of the rotational bands in nuclei with $Z \approx 100$ using a particle-number conserving method based on a cranked shell model

Zhen-Hua Zhang (张振华),[1] Xiao-Tao He (贺晓涛),[2] Jin-Yan Zeng (曾谨言),[3]
En-Guang Zhao (赵恩广),[1,3,4] and Shan-Gui Zhou (周善贵)[1,4,*]

[1]*State Key Laboratory of Theoretical Physics, Institute of Theoretical Physics, Chinese Academy of Sciences, Beijing 100190, China*
[2]*College of Material Science and Technology, Nanjing University of Aeronautics and Astronautics, Nanjing 210016, China*
[3]*School of Physics, Peking University, Beijing 100871, China*
[4]*Center of Theoretical Nuclear Physics, National Laboratory of Heavy Ion Accelerator, Lanzhou 730000, China*

(Received 27 October 2011; revised manuscript received 29 December 2011; published 25 January 2012)

The rotational bands in nuclei with $Z \approx 100$ are investigated systematically by using a cranked shell model (CSM) with the pairing correlations treated by a particle-number conserving (PNC) method, in which the blocking effects are taken into account exactly. By fitting the experimental single-particle spectra in these nuclei, a new set of Nilsson parameters (κ and μ) and deformation parameters (ε_2 and ε_4) are proposed. The experimental kinematic moments of inertia for the rotational bands in even-even, odd-A, and odd-odd nuclei, and the band-head energies of the one-quasiparticle bands in odd-A nuclei, are reproduced quite well by the PNC-CSM calculations. By analyzing the ω dependence of the occupation probability of each cranked Nilsson orbital near the Fermi surface and the contributions of valence orbitals in each major shell to the angular momentum alignment, the upbending mechanism in this region is understood clearly.

DOI: 10.1103/PhysRevC.85.014324 PACS number(s): 21.60.Cs, 21.10.Re, 23.20.Lv, 27.90.+b

I. INTRODUCTION

Since the importance of shell effects on the stability of superheavy nuclei (SHN) was illustrated [1] and the existence of an island of stability of SHN was predicted around $Z = 114$ and $N = 184$ [2–5], a lot of efforts have focused on the exploration of SHN. Great experimental progresses have been made in synthesizing the superheavy elements (SHE). Up to now, SHE's with $Z \leqslant 118$ have been synthesized via cold and hot fusion reactions [6–8]. However, these SHN are all neutron deficient with neutron numbers less by at least 7 than the predicted next neutron magic number 184. Therefore, one still cannot make a definite conclusion about the location of the island of stability.

The single particle shell structure is crucial for the location of the island of stability. For example, whether the next shell closure of protons appears at $Z = 114$ or 120 is mainly determined by the splitting of the spin doublets $\pi 2f_{5/2,7/2}$. Experimentally one cannot investigate directly the single particle level structure of SHN with $Z \geqslant 110$ because the production cross sections of these nuclei are tiny which makes the spectroscopy experiment impossible at present. Theoretically different models usually predict different closed shells beyond ^{208}Pb; even within the same model there are parameter-dependent predictions [9]. For examples, the macroscopic-microscopic models or the extended Thomas-Fermi-Strutinsky integral approach predict that the next shell closure for the proton is at $Z = 114$ [10–12]; the relativistic mean field models predict $Z = 114$ or 120 to be the next proton magic number [13–16]; predictions from nonrelativistic mean field models with Skyrme forces are $Z = 114$, 120, 124, or 126, depending on the parametrization [13]. The shell structure of SHN is important not only for the location of the island of stability, but also for the study of the synthesis mechanism of SHN [17–26], particularly for the survival probability of the excited compound nuclei [27,28].

To learn more about the shell structure of SHN, an indirect way is to study lighter nuclei in the deformed region with $Z \approx 100$ and $N \approx 152$. The strongly downsloping orbitals originating from the spherical subshells and active in the vicinity of the predicted shell closures may come close to the Fermi surface in these deformed nuclei. The rotational properties of nuclei in this mass region are affected strongly by these spherical orbitals. For examples, the $\pi 1/2^-[521]$ and $\pi 3/2^-[521]$ orbitals are of particular interest since they stem from the spherical spin doublets $\pi 2f_{5/2,7/2}$ orbitals.

Both the in-beam spectroscopy and spectroscopy following the decay of isomeric states or α decays have been used to study nuclei with $Z \approx 100$ [29–32]. These nuclei are well deformed; for example, the quadrupole deformation parameter $\beta_2 \approx 0.28$ for ^{250}Fm and ^{252,254}No [33–35]. Many high-spin rotational bands in even-even nuclei (e.g., ^{248,250,252}Cf [36], ^{250}Fm [34], ^{252,254}No [33,35]) and odd-A nuclei (e.g., ^{247,249}Cm and ^{249}Cf [37], ^{253}No [38,39], ^{251}Md [40], ^{255}Lr [41]) have been established in recent years. The study of these nuclei is certainly also very interesting in itself. The rotational spectra in these nuclei can reveal detailed information on the single-particle configurations, the shell structure, the stability against rotation, the high-K isomerism, etc.

Theoretically, the deformations, the shell structure, the rotational properties, and high-K isomeric states have been studied by using the self-consistent mean field models [42–45], the macroscopic-microscopic models [45–51], the projected shell model [52–54], the cranked shell models [55–57], the quasiparticle (qp) phonon model [58], the particle-triaxial-rotor

*sgzhou@itp.ac.cn

model [59], the heavy shell model [60], etc. Continuing the recently published Rapid Communication [57], in this work, we present results of a systematic study of the single particle structure and rotational properties of nuclei with $Z \approx 100$. The cranked shell model (CSM) with pairing correlations treated by a particle-number conserving (PNC) method [61,62] is used. In contrary to the conventional Bardeen-Cooper-Schrieffer (BCS) or Hartree-Fock-Bogoliubov (HFB) approach, in the PNC method, the Hamiltonian is solved directly in a truncated Fock space [63]. So the particle-number is conserved and the Pauli blocking effects are taken into account exactly. Note that the PNC scheme has been implemented both in relativistic and nonrelativistic mean field models [64, 65] in which the single-particle states are calculated from self-consistent mean field potentials instead of the Nilsson potential.

The paper is organized as follows. A brief introduction of the PNC treatment of pairing correlations within the CSM and applications of the PNC-CSM are presented in Sec. II. The numerical details, including a new set of Nilsson parameters (κ, μ), the deformation parameters, and pairing parameters are given in Sec. III. The PNC-CSM calculation results for even-even, odd-A, and odd-odd nuclei are presented in Sec. IV. A brief summary is given in Sec. V.

II. THEORETICAL FRAMEWORK

The cranked Nilsson Hamiltonian of an axially symmetric nucleus in the rotating frame reads [62,66]

$$H_{\rm CSM} = H_0 + H_{\rm P} = H_{\rm Nil} - \omega J_x + H_{\rm P} \,, \tag{1}$$

where $H_{\rm Nil}$ is the Nilsson Hamiltonian [4], $-\omega J_x$ is the Coriolis interaction with the cranking frequency ω about the x axis (perpendicular to the nuclear symmetry z axis). $H_{\rm P} = H_{\rm P}(0) + H_{\rm P}(2)$ is the pairing interaction:

$$H_{\rm P}(0) = -G_0 \sum_{\xi\eta} a^\dagger_\xi a^\dagger_{\bar\xi} a_{\bar\eta} a_\eta \,, \tag{2}$$

$$H_{\rm P}(2) = -G_2 \sum_{\xi\eta} q_2(\xi) q_2(\eta) a^\dagger_\xi a^\dagger_{\bar\xi} a_{\bar\eta} a_\eta \,, \tag{3}$$

where $\bar\xi$ $(\bar\eta)$ labels the time-reversed state of a Nilsson state ξ (η), $q_2(\xi) = \sqrt{16\pi/5}\langle\xi|r^2 Y_{20}|\xi\rangle$ is the diagonal element of the stretched quadrupole operator, and G_0 and G_2 are the effective strengths of monopole and quadrupole pairing interactions, respectively.

Instead of the usual single-particle level truncation in common shell-model calculations, a cranked many-particle configuration (CMPC) truncation (Fock space truncation) is adopted which is crucial to make the PNC calculations for low-lying excited states both workable and sufficiently accurate [63,67]. An eigenstate of $H_{\rm CSM}$ can be written as

$$|\psi\rangle = \sum_i C_i |i\rangle, \quad (C_i \text{ real}) \,, \tag{4}$$

where $|i\rangle$ is a CMPC (an eigenstate of the one-body operator H_0). By diagonalizing $H_{\rm CSM}$ in a sufficiently large CMPC space, sufficiently accurate solutions for low-lying excited eigenstates of $H_{\rm CSM}$ are obtained.

The angular momentum alignment of $|\psi\rangle$ can be separated into the diagonal and the off-diagonal parts,

$$\langle\psi|J_x|\psi\rangle = \sum_i C_i^2 \langle i|J_x|i\rangle + 2\sum_{i<j} C_i C_j \langle i|J_x|j\rangle \,, \tag{5}$$

and the kinematic moment of inertia (MOI) of $|\psi\rangle$ is

$$J^{(1)} = \frac{1}{\omega}\langle\psi|J_x|\psi\rangle \,. \tag{6}$$

Considering J_x to be a one-body operator, the matrix element $\langle i|J_x|j\rangle$ for $i \neq j$ is nonzero only when $|i\rangle$ and $|j\rangle$ differ by one particle occupation [62,68]. After a certain permutation of creation operators, $|i\rangle$ and $|j\rangle$ can be recast into

$$|i\rangle = (-1)^{M_{i\mu}}|\mu\cdots\rangle \,, \quad |j\rangle = (-1)^{M_{j\nu}}|\nu\cdots\rangle \,, \tag{7}$$

where the ellipsis stands for the same particle occupation, and $(-1)^{M_{i\mu}} = \pm 1$, $(-1)^{M_{j\nu}} = \pm 1$ according to whether the permutation is even or odd. Therefore, the kinematic MOI of $|\psi\rangle$ can be written as

$$J^{(1)} = \sum_\mu j^{(1)}_\mu + \sum_{\mu<\nu} j^{(1)}_{\mu\nu} \,, \tag{8}$$

where

$$j^{(1)}_\mu = \frac{n_\mu}{\omega}\langle\mu|j_x|\mu\rangle \,,$$

$$j^{(1)}_{\mu\nu} = \frac{2}{\omega}\langle\mu|j_x|\nu\rangle \sum_{i<j}(-1)^{M_{i\mu}+M_{j\nu}} C_i C_j \,, \quad (\mu \neq \nu) \,,$$

and

$$n_\mu = \sum_i |C_i|^2 P_{i\mu} \,, \tag{9}$$

is the occupation probability of the cranked orbital $|\mu\rangle$, $P_{i\mu} = 1$ if $|\mu\rangle$ is occupied in $|i\rangle$, and $P_{i\mu} = 0$ otherwise.

We note that because $R_x(\pi) = e^{-i\pi J_x}$, $[J_x, J_z] \neq 0$, the signature scheme breaks the quantum number K. However, it has been pointed out that [62,69], although $[J_x, J_z] \neq 0$, $[R_x(\pi), J_z^2] = 0$. Thus we can construct simultaneous eigenstates of $(R_x(\pi), J_z^2)$. Each CMPC $|i\rangle$ in Eq. (4) is chosen as a simultaneous eigenstate of (H_0, J_z^2). It should be noted that, though the projection K of the total angular momentum of a deformed spheroidal nucleus is a constant of motion, K can not keep constant when the rotational frequency ω is nonzero due to the Coriolis interaction. However, in the low-ω region, K may be served as a useful quantum number characterizing a low-lying excited rotational band.

The PNC-CSM treatment has been used to describe successfully the high-spin states of the normally deformed nuclei in the rare-earth and the actinide regions, and the superdeformed nuclei in $A \approx 190$ region. The multi-qp high-K isomeric states are investigated in detail in the well-deformed Lu ($Z = 71$), Hf ($Z = 72$) and Ta ($Z = 73$) isotopes [70,71]. The backbendings in Yb ($Z = 70$) and Tm ($Z = 68$) isotopes are understood clearly, especially the occurrence of sharp backbending in some nuclei [72,73]. The upbending mechanisms in the actinide nuclei ^{251}Md and ^{253}No are also analyzed [56]. In the superdeformed nuclei around $A \approx 190$ region, the effects

of the quadrupole pairing on the downturn of dynamic MOI's are analyzed [66], the evolution of the dynamic MOI's and the alignment additivity, which come from the contributions of the interference terms, have been investigated [74].

Some general features in nuclear structure physics have also been explained well in the PNC-CSM scheme, e.g., the large fluctuations of odd-even differences in MOI's [68], the nonadditivity in MOI's [75], the microscopic mechanism of identical bands in normally deformed and superdeformed nuclei [76,77], the nonexistence of the pairing phase transition [78], etc.

In Ref. [57], the high-spin rotational bands in ^{247,249}Cm and ^{249}Cf established in Ref. [37] have been calculated using the PNC-CSM method and the upbending mechanism is discussed. This paper is an extension of [57], providing more details and a systematic investigation of nuclei with $Z \approx 100$.

III. NUMERICAL DETAILS

A. A new set of Nilsson parameters

The conventional Nilsson parameters (κ, μ) proposed in Refs. [4,79] are optimized to reproduce the experimental level schemes for the rare-earth and actinide nuclei. However, these two sets of parameters cannot describe well the experimental level schemes of nuclei studied in this work. By fitting the experimental single-particle levels in the odd-A nuclei with $Z \approx 100$, we obtained a new set of Nilsson parameters (κ, μ) which are dependent on the main oscillator quantum number N as well as the orbital angular momentum l [57]. Here for the completeness, we include them again in Table I. Note that the readjustment of Nilsson parameters is also necessary in some other mass regions of the nuclear chart [80–82] and the l dependence was already included in Refs. [80,81].

B. Deformation parameters

There are not enough experimental values of the deformation parameters for the very heavy nuclei with $Z \approx 100$. According to the data, the quadrupole deformation parameter $\beta_2 \approx 0.28 \pm 0.02$ for ^{250}Fm [34], ^{252,254}No [35]. The values used in various calculations or predicted by different models are quite different. Figure 1 shows the experimental quadrupole deformation (pink stars in Fig. 1) and those predicted in some macroscopic-microscopic (MM) models [46,48] (blue triangles in Fig. 1) and the finite range droplet model (FRDM) [11] (red solid circles in Fig. 1). The

TABLE I. Nilsson parameters κ and μ proposed for the nuclei with $Z \approx 100$, which has been given in Ref. [57].

N	l	κ_p	μ_p	N	l	κ_n	μ_n
4	0,2,4	0.0670	0.654				
5	1	0.0250	0.710	6	0	0.1600	0.320
	3	0.0570	0.800		2	0.0640	0.200
	5	0.0570	0.710		4,6	0.0680	0.260
6	0,2,4,6	0.0570	0.654	7	1,3,5,7	0.0634	0.318

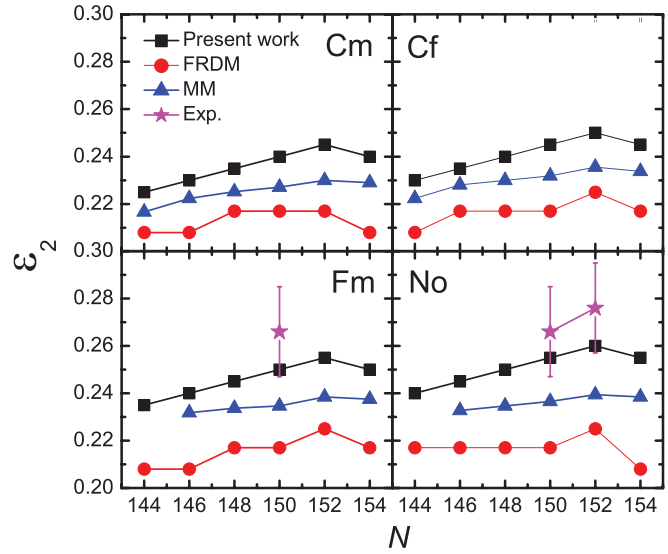

FIG. 1. (Color online) The quadrupole deformations given in Table II (black squares) and those predicted by a macroscopic-microscopic (MM) model [46,48] (blue triangles) and the finite range droplet model (FRDM) [11] (red solid circles). The experimental values for ^{250}Fm [34] and ^{252,254}No [35] (pink stars) are also shown for comparison.

deformation parameters given in these two MM models [46,48] are very close to each other, hence we only show the results given in Ref. [48]. From Fig. 1 we can see that the deformation parameters from MM and FRDM do not agree with the experimental values, especially those from the FRDM. One can find a general trend in Fig. 1, i.e., both the experimental values and the predicted values indicate that the deformations reach maximum at ^{254}No ($Z = 102$ and $N = 152$) partly according to which we fix the deformation parameters used in the present study.

The deformations are input parameters in the PNC-CSM calculations (black squares in Fig. 1). They are chosen to be close to existed experimental values and change smoothly according to the proton and the neutron number. The deformation parameters ε_2 and ε_4 used in our PNC-CSM calculations for even-even nuclei with $Z \approx 100$ are listed in Table II. The deformations of odd-A and odd-odd nuclei are taken as the average of the neighboring even-even nuclei. These parameters we choose may have some discrepancy from the empirical values which may lead to some deviations in the single-particle levels if they are very close to each other. For example, the level sequence of the 1-qp bands will change in an isotonic or an isotopic chain (e.g., see Figs. 6 and 11) due to the deformation staggering in the neighboring nuclei. From Fig. 1 it can be seen that this staggering existed in the FRDM. Some previous calculations have shown that the octupole correlations play important roles in this mass region [53,83,84]. In the present work, the octupole deformation is not included yet. We note that the octupole effect may modify the single-particle level scheme. One example will be discussed later for the low excitation energy of the $\nu 5/2^+[622]$ states in the $N = 151$ isotones in Sec. IV B.

TABLE II. Deformation parameters ε_2 and ε_4 used in the PNC-CSM calculations for even-even nuclei with $Z \approx 100$.

N	144	146	148	150	152	154
$Z = 96$	^{240}Cm	^{242}Cm	^{244}Cm	^{246}Cm	^{248}Cm	^{250}Cm
ε_2	0.225	0.230	0.235	0.240	0.245	0.240
ε_4	−0.015	−0.010	−0.005	0.000	0.005	0.01
$Z = 98$	^{242}Cf	^{244}Cf	^{246}Cf	^{248}Cf	^{250}Cf	^{252}Cf
ε_2	0.230	0.235	0.240	0.245	0.250	0.245
ε_4	−0.01	−0.005	0.000	0.005	0.010	0.015
$Z = 100$	^{244}Fm	^{246}Fm	^{248}Fm	^{250}Fm	^{252}Fm	^{254}Fm
ε_2	0.235	0.240	0.245	0.250	0.255	0.250
ε_4	−0.005	0.000	0.005	0.010	0.015	0.02
$Z = 102$	^{246}No	^{248}No	^{250}No	^{252}No	^{254}No	^{256}No
ε_2	0.240	0.245	0.250	0.255	0.260	0.255
ε_4	0	0.005	0.010	0.015	0.020	0.025

C. Pairing strengths and the CMPC space

The effective pairing strengths G_0 and G_2 can be determined by the odd-even differences in nuclear binding energies. They are connected with the dimension of the truncated CMPC space. The CMPC space for the heavy nuclei studied in this work is constructed in the proton $N = 4, 5, 6$ shells and the neutron $N = 6, 7$ shells. The dimensions of the CMPC space for the nuclei with $Z \approx 100$ are about 1000 both for protons and neutrons. The corresponding effective monopole and quadrupole pairing strengths are shown in Table III. As we are only interested in the yrast and low-lying excited states, the number of the important CMPC's involved (weight >1%) is not very large (usually <20) and almost all the CMPC's with weight >0.1% are included in.

The stability of the PNC calculation results against the change of the dimension of the CMPC space has been investigated in Refs. [62,67,77]. A larger CMPC space with renormalized pairing strengths gives essentially the same results. The calculated MOI's of the ground state band (GSB) in ^{248}Cm using different dimensions of the CMPC space (1000 and 1500, respectively) are compared in Fig. 2. The red dotted line is the result calculated with the dimensions of CMPC space about 1500 both for protons and neutrons. The effective pairing strengths used in the calculation are $G_p = 0.35$ MeV, $G_{2p} = 0.03$ MeV, $G_n = 0.27$ MeV, and $G_{2n} = 0.013$ MeV, which are a little smaller than those used when the CMPC dimensions are about 1000, i.e., $G_p = 0.40$ MeV, $G_{2p} = 0.035$ MeV, $G_n = 0.30$ MeV, and $G_{2n} = 0.020$ MeV (see Table III). We can see that these two results agree well with each other and they both also agree well with the experiment. So the solutions to the low-lying excited states are quite satisfactory.

TABLE III. Effective pairing strengths used in the PNC-CSM calculations for the nuclei with $Z \approx 100$.

	even-even	odd-N	odd-Z	odd-odd
G_{0p} (MeV)	0.40	0.40	0.25	0.25
G_{2p} (MeV)	0.035	0.035	0.010	0.010
G_{0n} (MeV)	0.30	0.25	0.30	0.25
G_{2n} (MeV)	0.020	0.015	0.020	0.015

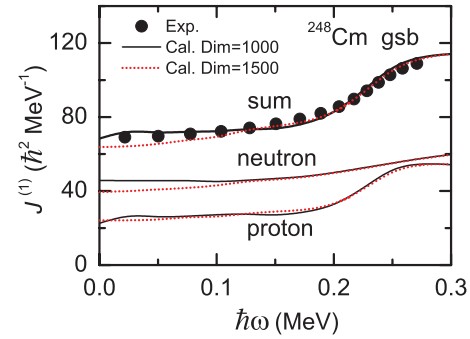

FIG. 2. (Color online) The calculated MOI's of the GSB in ^{248}Cm using different dimensions of the CMPC space [1000 (black solid lines) and 1500 (red dotted lines), respectively]. The experimental values are denoted by solid circles. The effective pairing strengths used in the calculation, when the dimension is 1500 (1000), are $G_p = 0.35$ MeV, $G_{2p} = 0.03$ MeV, $G_n = 0.27$ MeV, $G_{2n} = 0.013$ MeV ($G_p = 0.40$ MeV, $G_{2p} = 0.035$ MeV, $G_n = 0.30$ MeV, $G_{2n} = 0.020$ MeV as given in Table III).

IV. RESULTS AND DISCUSSIONS

A. Cranked Nilsson levels

Figure 3 shows the calculated cranked Nilsson levels near the Fermi surface of ^{250}Fm. The positive (negative) parity levels are denoted by blue (red) lines. The signature $\alpha = +1/2$ ($\alpha = -1/2$) levels are denoted by solid (dotted) lines. For protons, the sequence of single-particle levels near the Fermi surface is exactly the same as that determined from the experimental information of ^{249}Es [31]. The sequence of single-neutron levels near the Fermi surface is also very consistent with the one determined from the experimental information of ^{251}Fm [31], with the only exception of the $\nu 5/2^+[622]$ orbital which will be discussed in next subsection.

From Fig. 3 it is seen that there exist a proton gap at $Z = 100$ and a neutron gap at $N = 152$, which is consistent with

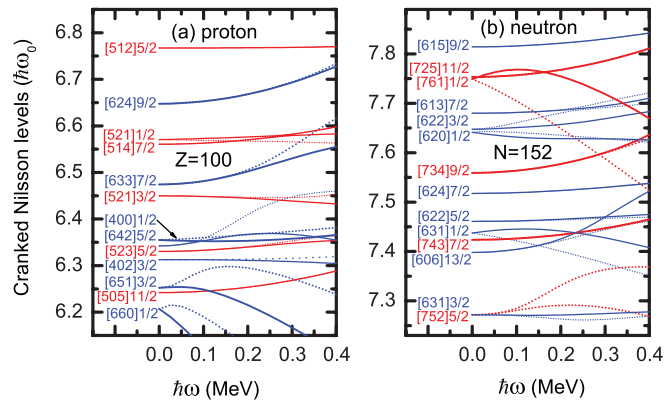

FIG. 3. (Color online) The cranked Nilsson levels near the Fermi surface of ^{250}Fm (a) for protons and (b) for neutrons. The positive (negative) parity levels are denoted by blue (red) lines. The signature $\alpha = +1/2$ ($\alpha = -1/2$) levels are denoted by solid (dotted) lines.

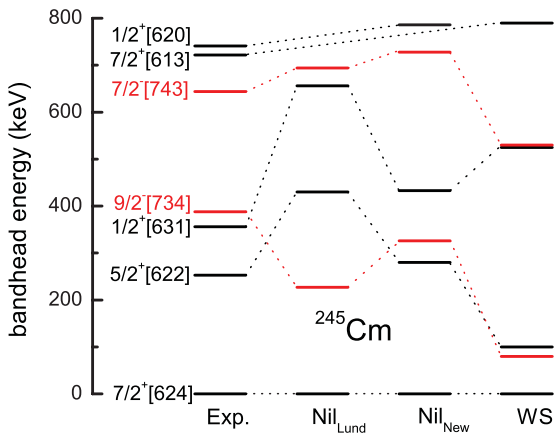

FIG. 4. (Color online) Comparison between experimental and theoretical 1-qp band-head energies for ^{245}Cm. The Lund systematic Nilsson parameters are taken from [4]. The results using Woods-Saxon potential are taken from [50]. The positive and negative parity states are denoted by black and red lines, respectively.

the experiment and the calculation by using a Woods-Saxon potential [85]. The position of the proton orbitals $1/2^-[521]$ and $3/2^-[521]$ is very important, because they stem from the spherical spin partners $2f_{5/2,7/2}$ orbitals. The magnitude of the spin-orbital splitting of these spin partners determines whether the next proton magic number is $Z = 114$ or 120. Note that the cranked relativistic Hartree-Bogoliubov theory has been used to investigate the spin-orbital splitting of this spin partners in Ref. [42]. The calculated proton levels indicate that the $Z = 120$ gap is large whereas the $Z = 114$ gap is small.

The neutron $1/2^+[620]$ orbital is the highest-lying neutron orbital from above the $N = 164$ spherical subshell ($2g_{7/2}$), based on which a high-spin rotational band has been established in ^{249}Cm [37]. This orbital also brings new information toward studying those states close to the next closed shell for neutrons.

B. 1-qp band-head energies

First we choose ^{245}Cm as an example to show the comparison of theoretical 1-qp band-head energies with the data in Fig. 4. It can be seen that the calculated results obtained by using the conventional Nilsson parameters [4] deviate from the experimental values very much. With the modified parameters given in Table I, a remarkably good agreement with the data can be achieved. For comparison, the results from the Woods-Saxon (WS) potential [50] is also given (the band-head energies are taken from Table II of Ref. [50] except that that of $7/2^+[613]$ is taken from Fig. 1 of the same article). It should be noted that generally speaking, for the 1-qp spectra of nuclei with $Z \approx 100$ the Woods-Saxon potential gives a better agreement with the data. For example, the root-mean-square deviation of theoretical 1-qp band-head energies from the experimental values is about 270 keV for neutrons by using the modified Nilsson parameters, while this deviation is about 200 keV by using the Woods-Saxon potential [50].

Figures 5–12 show experimental and calculated band-head energies of the low-lying 1-qp bands for even-Z and odd-N isotones with $N = 145 - 153$ (one-quasineutron states) and odd-Z and even-N isotopes with $Z = 97$–103 (one-quasiproton states). In these figures, 1-qp states with energies around or less than 0.8 MeV are shown and the positive and negative parity states are denoted by black and red lines, respectively. Generally speaking, the agreement between the calculation and the experiment is satisfactory. Next we discuss these 1-qp states in details.

The experimental and calculated band-head energies of low-lying one-quasineutron bands for the $N = 145$ isotones are compared in Fig. 5. The data are available only for ^{241}Cm [86] and ^{243}Cf [87] and they are reproduced by the theory quite well. The ground state of each $N = 145$ isotone studied in this work is $\nu 1/2^+[631]$. The energy of $\nu 5/2^+[622]$ steadily becomes smaller with Z increasing both in the experimental spectra and in the calculated ones. The lowering of $\nu 7/2^+[624]$ with Z increasing is also seen in the experimental spectra but it is not so striking from the calculation. In each of these isotones a low-lying state $\nu 7/2^-[743]$ is predicted which is not observed. We note that this prediction is consistent with Ref. [50].

Low-lying one-quasineutron levels for $N = 147$ isotones ^{243}Cm [88], ^{245}Cf [87], and ^{247}Fm [89] were identified experimentally. Their ground states are $\nu 5/2^+[622]$, $\nu 1/2^+[631]$, and $\nu 7/2^+[624]$ respectively. However, the

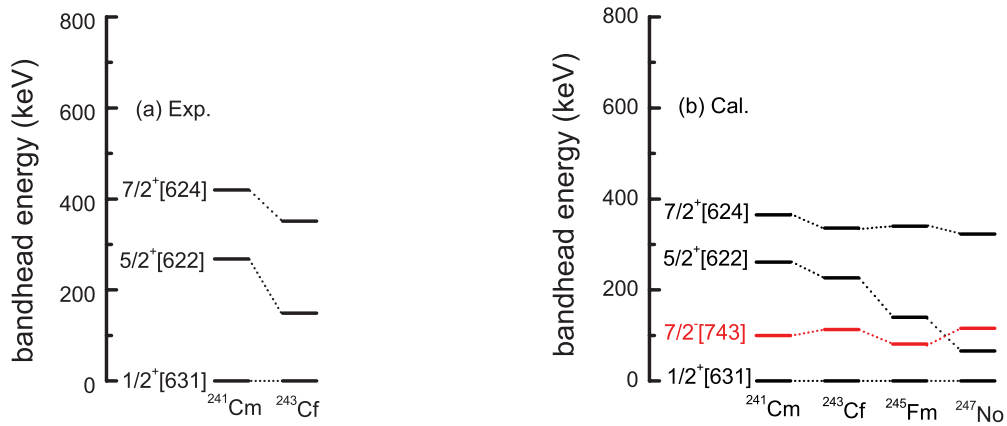

FIG. 5. (Color online) (a) Experimental and (b) calculated band-head energies of low-lying one-quasineutron bands for the $N = 145$ isotones. The data are taken from [86,87]. The positive and negative parity states are denoted by black and red lines, respectively.

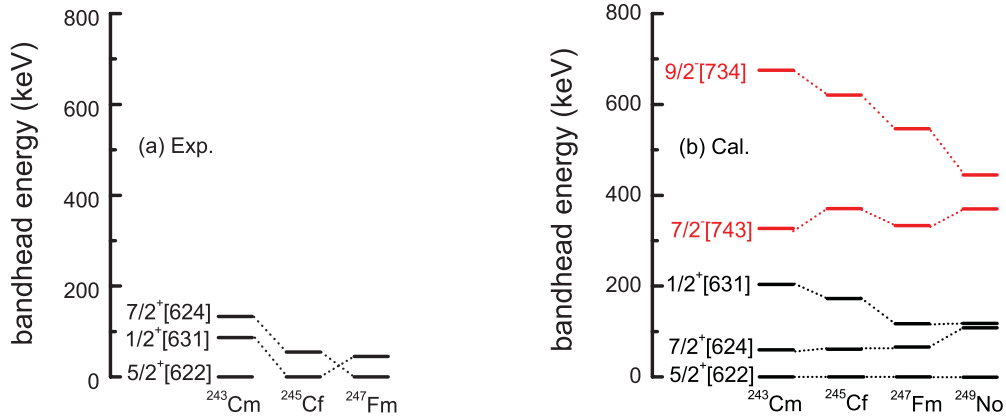

FIG. 6. (Color online) (a) Experimental and (b) calculated band-head energies of low-lying one-quasineutron bands for the $N = 147$ isotones. The data are taken from [87–89]. The positive and negative parity states are denoted by black and red lines, respectively.

ground state for all these isotones is $\nu 5/2^+[622]$ from the PNC-CSM as seen in Fig. 6. The same is obtained recently by using a two-center shell model [45]. In our calculations, the energies of these three levels are very close to each other, a small change in the deformation parameters would modify the order of these levels. This might be one of the reasons for the disagreement in the ground state configuration between the theory and the experiment. Similar situation happens in the Bk and Es isotopes, in which the energies of $\pi 3/2^-[521]$ and $\pi 7/2^+[633]$ are very close to each other and these two one-quasiproton levels cross each other at $N = 152$.

Low-lying one-quasineutron levels for $N = 149$ isotones ^{245}Cm [90], ^{247}Cf [91], ^{249}Fm [92] and ^{251}No [89] were identified experimentally. All their ground states are $\nu 7/2^+[624]$. The comparison with the experiment is shown in Fig. 7. Nearly all of these 1-quasineutron band-head energies are well reproduced by the PNC-CSM calculations. The energy of $\nu 1/2^+[631]$ is much lower in ^{251}No than that in ^{245}Cm, but in our calculations this level seems almost unchange with the proton number increasing. The calculated results are very similar with that in Ref. [93]. For each observed level, the energy reaches maximum in ^{247}Cf, which can not be reproduced by our calculations.

Many theoretical models predict that the first excited state in $N = 151$ isotones should be $\nu 7/2^+[624]$ (see, e.g., Ref. [50]). This is not consistent with experimental results, i.e., the first excited state in $N = 151$ isotones is $\nu 5/2^+[622]$. The low excitation energy of the $\nu 5/2^+[622]$ states in the $N = 151$ isotones have been interpreted as a consequence of the presence of a low-lying $K^\pi = 2^-$ octupole phonon state [97]. Noted that in Ref. [42], by using the cranked relativistic Hartree-Bogoliubov theory, the level sequence in $N = 151$ isotones is consistent with the experiment, but it can not reproduce the level sequence in $N = 149$ isotones. It can be seen in Fig. 8 that, the level sequence in most nuclei is consistent with the experimental data, with an obvious exception of the $\nu 5/2^+[622]$ orbital. The level $\nu 7/2^+[624]$ observed in ^{253}No at 355 keV is taken from Ref. [38]. A recent experiment [39] observed a very similar level scheme which was, however, assigned as the $\nu 7/2^-[734]$ configuration. This will be discussed in Sec. IV.

The experimental and calculated band-head energies of low-lying one-quasineutron bands for the $N = 153$ isotones are compared in Fig. 9. The one-quasineutron levels for ^{249}Cm [98], ^{251}Cf [99], ^{253}Fm [100], and ^{255}No [101] were identified experimentally. The ground states for all these isotones are

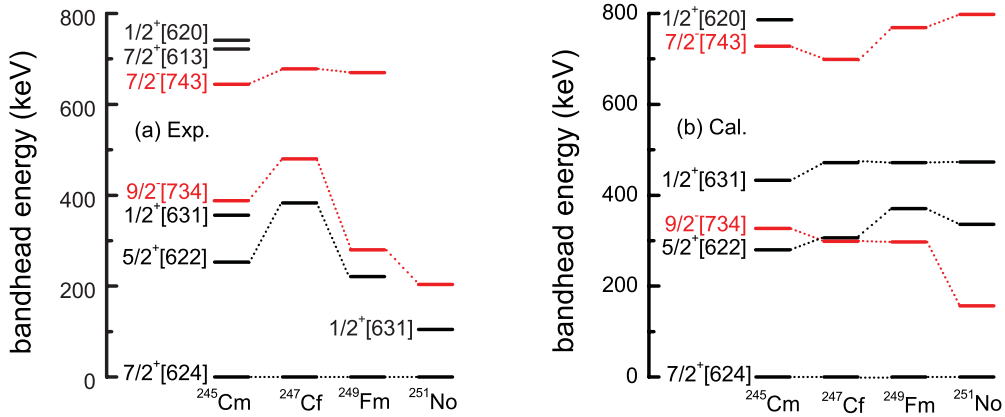

FIG. 7. (Color online) (a) Experimental and (b) calculated band-head energies of low-lying one-quasineutron bands for the $N = 149$ isotones. The data are taken from [89–92]. The positive and negative parity states are denoted by black and red lines, respectively.

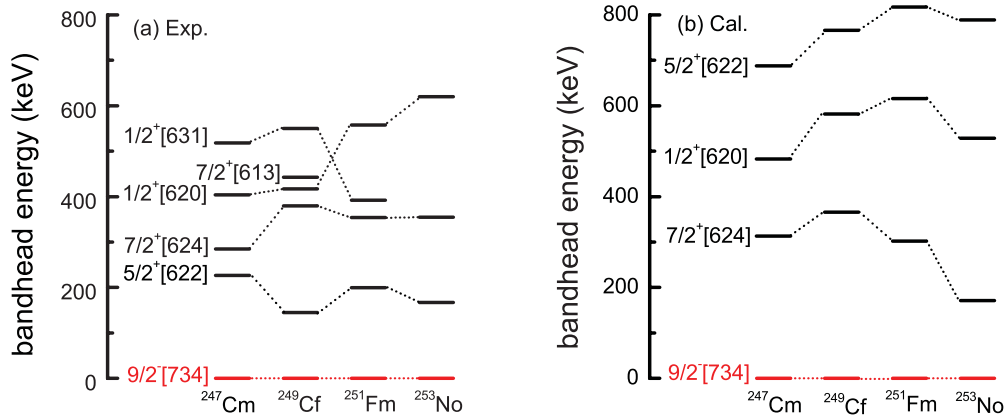

FIG. 8. (Color online) (a) Experimental and (b) calculated band-head energies of low-lying one-quasineutron bands for the $N = 151$ isotones. The data are taken from [93–96]. The configuration assignment $7/2^+[624]$ in ^{253}No are taken from Ref. [38] and discussed in Sec. IV. The positive and negative parity states are denoted by black and red lines, respectively.

$\nu 1/2^+[620]$ in our calculations, which is consistent with the data. But the level order of $\nu 7/2^+[613]$ and $\nu 3/2^+[622]$ from our calculation is inversed according to the data. This also happens in Ref. [50]. Another problem is that $\nu 11/2^-[725]$ states in all the isotones from our calculation are systematically higher than the experimental values. In each of these isotones a low-lying state $\nu 7/2^-[743]$ is predicted which is not observed.

Low-lying one-quasiproton levels for Bk ($Z = 97$) isotopes ^{243,245}Bk [102], ^{247}Bk [103], ^{249}Bk [104], and ^{251}Bk [105] were identified experimentally. The comparison between the data and our calculation is shown in Fig. 10. The two levels $\pi 3/2^-[521]$ and $\pi 7/2^+[633]$ are very close to each other, usually the energy difference is less than 50 keV. The ground states are $\pi 3/2^-[521]$ for all Bk isotopes except ^{249}Bk. In our calculations the ground states are all $\pi 3/2^-[521]$. The deviation in ^{249}Bk may be due to the staggering of the deformation. Nearly all the calculated one-quasiproton energies in the Bk isotopes are a little larger than the experimental values.

Low-lying one-quasineutron levels for Es ($Z = 99$) isotopes ^{245,247,249,251,253}Es [106,107] were identified experimentally. The comparison between the data and our calculation is shown in Fig. 11. The ground states are $\pi 7/2^+[633]$ for all Es isotopes except ^{251}Es. In our calculations the ground states are all $\pi 7/2^+[633]$. The deviation in ^{251}Es may be also due to the staggering of the deformation. Our calculations show that the band-head energies of the negative parity states are all very small (less than 400 keV), which is consistent with the experiment.

With the proton number increasing, the data become less and less. Figure 12 shows the comparison between the experimental values and our calculation for the Md and Lr isotopes. The data are available only for ^{251}Md [109], ^{255}Md [108], and ^{251}Lr [109] and they are reproduced by the theory quite well.

From the above discussions, we see that the new Nilsson parameters can describe satisfactorily the 1-qp spectra of nuclei with $Z \approx 100$. But there are still some discrepancies. According to our experience, it is quite difficult to improve this situation in the framework of the Nilsson model. One way out might be to use the Woods-Saxon potential instead of the Nilsson potential.

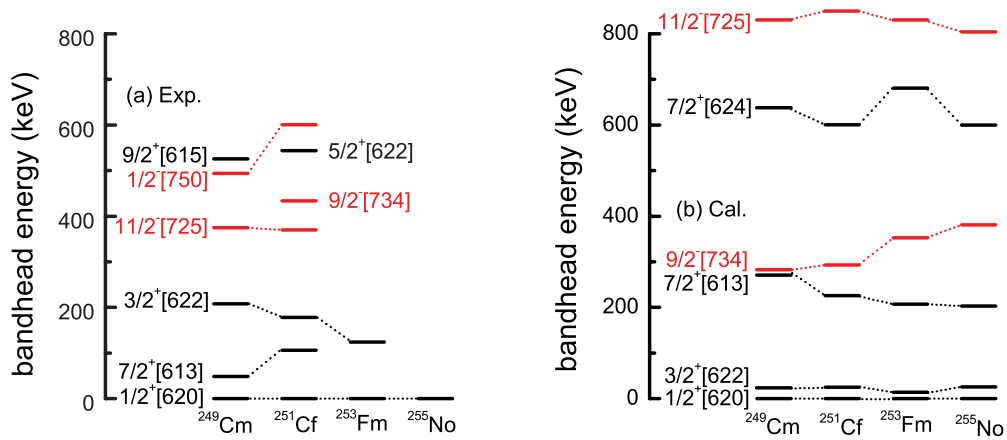

FIG. 9. (Color online) (a) Experimental and (b) calculated bandhead energies of low-lying one-quasineutron bands for the $N = 153$ isotones. The data are taken from [98–101]. The positive and negative parity states are denoted by black and red lines, respectively.

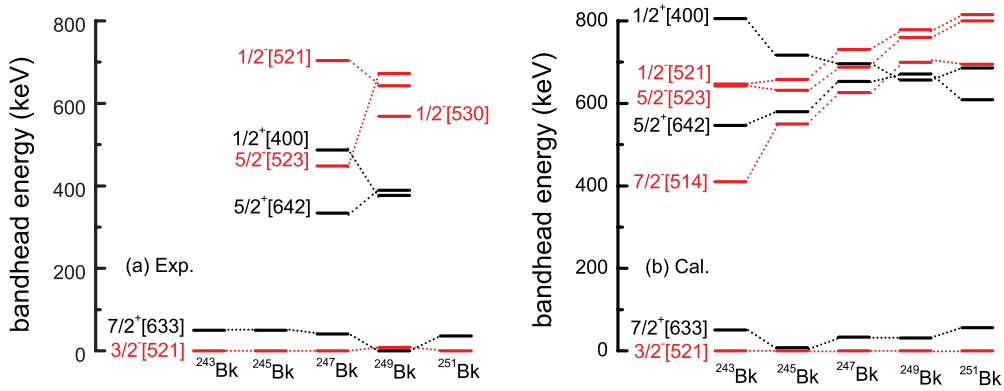

FIG. 10. (Color online) (a) Experimental and (b) calculated band-head energies of low-lying one-quasiproton bands for the Bk ($Z = 97$) isotopes. The data are taken from [102–105]. The positive and negative parity bands are denoted by black and red lines, respectively.

C. Even-even nuclei

The experimental kinematic MOI's for each band are extracted by

$$\frac{J^{(1)}(I)}{\hbar^2} = \frac{2I+1}{E_\gamma(I+1 \to I-1)}, \tag{10}$$

separately for each signature sequence within a rotational band. The relation between the rotational frequency ω and the angular momentum I is

$$\hbar\omega(I) = \frac{E_\gamma(I+1 \to I-1)}{I_x(I+1) - I_x(I-1)}, \tag{11}$$

where $I_x(I) = \sqrt{(I+1/2)^2 - K^2}$, K is the projection of nuclear total angular momentum along the symmetry z axis of an axially symmetric nuclei.

Figure 13 shows the experimental and calculated MOI's of the GSB's in even-even Cm, Cf, Fm, and No isotopes. The experimental (calculated) MOI's are denoted by solid circles (solid lines). The experimental MOI's of all these GSB's are well reproduced by the PNC-CSM calculations. For some nuclei, there is no data (e.g., ^{252}Cm), we only show the PNC-CSM results. It can be seen from Fig. 13 that with increasing proton number Z in any isotonic chain, the upbendings in each nuclei become less pronounced. It is well known that the backbending is caused by the crossing of the GSB with a pair-broken band based on high-j intruder orbitals [110], in this mass region the $\pi i_{13/2}$ and $\nu j_{15/2}$ orbitals. But in several nuclei, there is no evidence for a $\nu j_{15/2}$ alignment. It has been pointed out in Ref. [57] that, for the nuclei with $N \approx 150$, among the neutron orbitals of $j_{15/2}$ parentage, only the high-Ω (deformation aligned) $\nu 7/2^-[743]$ and $\nu 9/2^-[734]$ are close to the Fermi surface. The diagonal parts in Eq. (5) of these two orbitals contribute no alignment to the upbending, only the off-diagonal parts in Eq. (5) contribute a little if the neutron $j_{15/2}$ orbital is not blocked.

To see the upbending in these even-even nuclei more clearly, we show the experimental (solid circles) and calculated (solid lines) alignment i for the GSB's in $N = 150$ isotones in Fig. 14. For other isotones the results are very similar, so we do not shown them here. It can be seen that the upbending frequencies of these GSB's are about $0.20 \sim 0.25$ MeV.

One of the advantages of the PNC method is that the total particle number $N = \sum_\mu n_\mu$ is exactly conserved, whereas the occupation probability n_μ for each orbital varies with rotational frequency $\hbar\omega$. By examining the ω dependence of the orbitals close to the Fermi surface, one can learn more about how the Nilsson levels evolve with rotation and get some insights on the upbending mechanism. Figure 15 shows the occupation probability n_μ of each orbital μ near the Fermi surface for the GSB's in the $N = 150$ isotones. The top and bottom rows are for the protons and neutrons, respectively. The

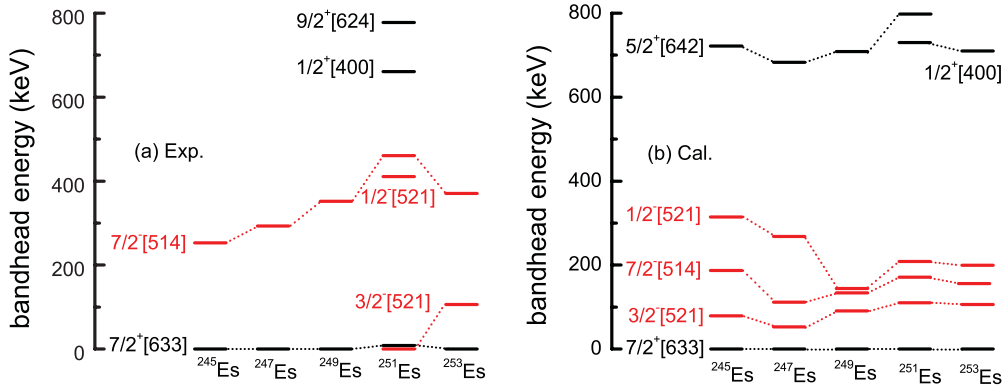

FIG. 11. (Color online) (a) Experimental and (b) calculated band-head energies of low-lying one-quasiproton bands for the Es ($Z = 99$) isotopes. The data are taken from [106,107]. The positive and negative parity states are denoted by black and red lines, respectively.

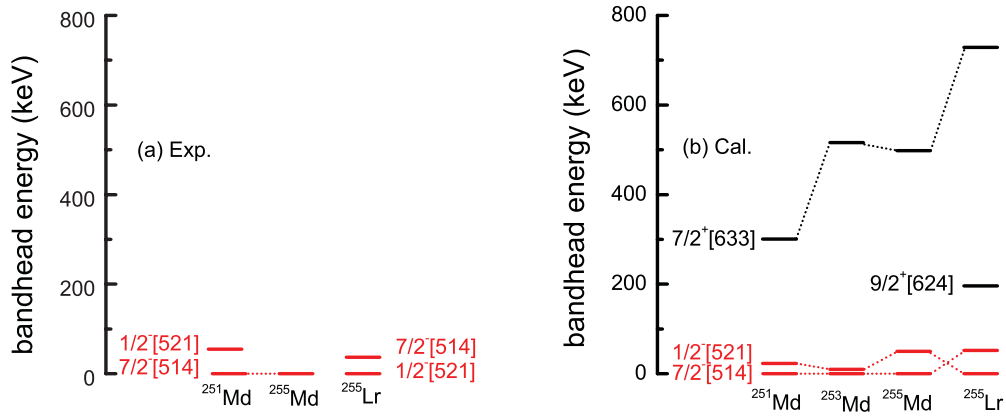

FIG. 12. (Color online) (a) Experimental and (b) calculated band-head energies of low-lying one-quasiproton bands for the Md ($Z = 101$) and Lr ($Z = 103$) isotopes. The data are taken from [108,109]. The positive and negative parity states are denoted by black and red lines, respectively.

positive (negative) parity levels are denoted by blue solid (red dotted) lines. The orbitals in which n_μ do not change much (i.e., contribute little to the upbending) are denoted by black lines. The Nilsson levels far above the Fermi surface ($n_\mu \sim 0$) and far below ($n_\mu \sim 2$) are not shown. We can see from Fig. 15 that the occupation probability of $\pi 7/2^+[633]$ ($\pi i_{13/2}$) drops down gradually from 0.5 to nearly zero with the cranking frequency $\hbar\omega$ increasing from about 0.20 MeV to 0.30 MeV, while the occupation probabilities of some other orbitals slightly increase. This can be understood from the cranked Nilsson levels shown in Fig. 3. The $\pi 7/2^+[633]$ is slightly above the Fermi surface at $\hbar\omega = 0$ MeV. Due to the pairing correlations, this orbital is partly occupied. With increasing $\hbar\omega$, this orbital leaves farther above the Fermi surface. So after the band-crossing frequency, the occupation probability of this orbital becomes smaller with increasing $\hbar\omega$. Meanwhile, the occupation probabilities of those orbitals which approach near to the Fermi surface become larger with increasing $\hbar\omega$. This phenomenon is even more clear in ^{248}Cf, but the band crossing occurs at $\hbar\omega_c \sim 0.25$ MeV, a little larger than that of ^{246}Cm. So the band crossings in both cases are mainly caused by the $\pi i_{13/2}$ orbitals. For ^{250}Fm and ^{252}No, the occupation probabilities of $\pi i_{13/2}$ orbitals increase slowly with the cranking frequency $\hbar\omega$ increasing from about 0.20 MeV to 0.30 MeV. So there is no sharp band crossing from the proton orbitals. Now we focus on the occupation probability n_μ of the neutron orbitals (bottom row). The four figures in the bottom row of Fig. 15 show a very similar pattern. It can be seen that, with $\hbar\omega$ increasing, the n_μ of $\nu 7/2^+[624]$ orbitals increase slowly and that of the high-Ω (deformation aligned) $\nu 9/2^-[734]$

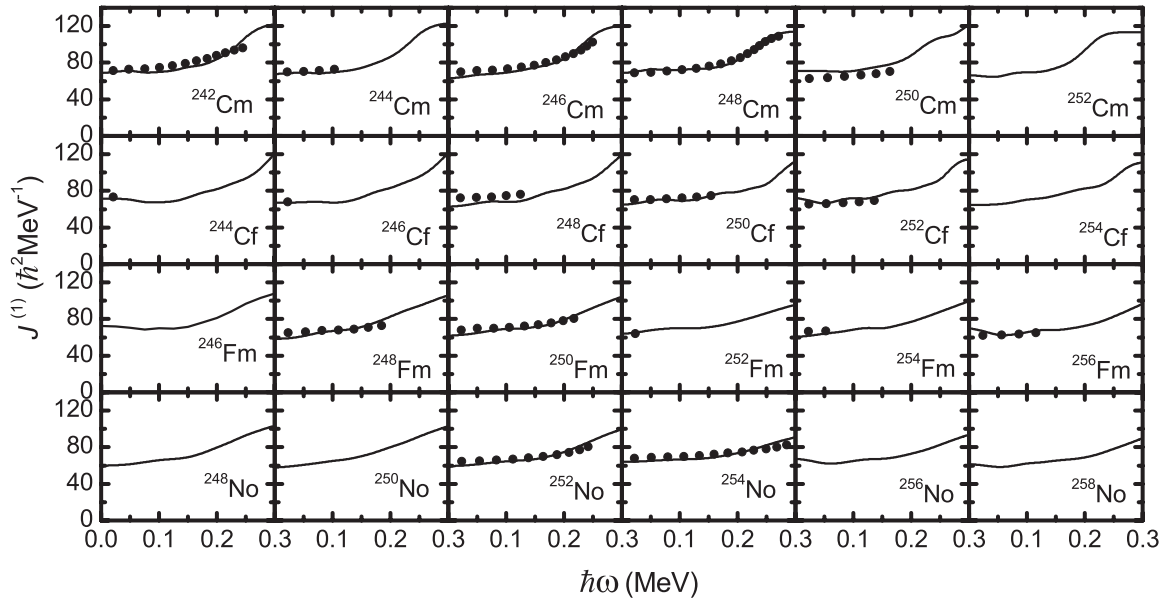

FIG. 13. The experimental (solid circles) and calculated (solid lines) MOI's $J^{(1)}$ for the GSB's in Cm, Cf, Fm, and No isotopes from $N = 146$ to $N = 156$. The data are taken from Ref. [31] and references therein. The most recent data of ^{248,250,252}Cf are taken from [36]. The effective pairing interaction strengths for all these even-even nuclei are, $G_n = 0.30$ MeV, $G_{2n} = 0.020$ MeV, $G_p = 0.40$ MeV, and $G_{2p} = 0.035$ MeV.

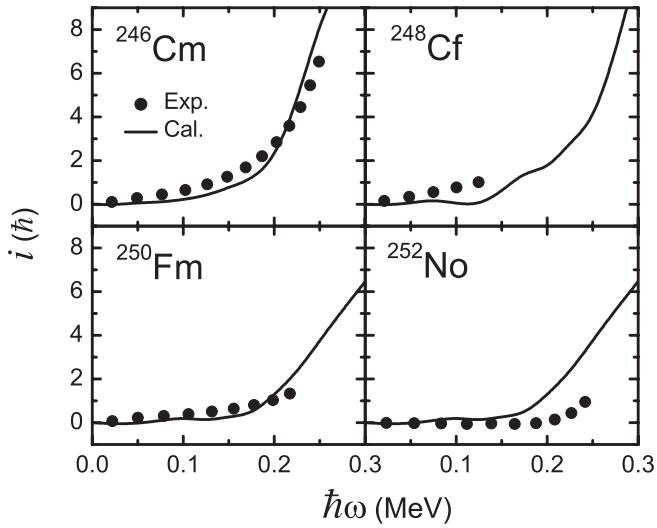

FIG. 14. The experimental (solid circles) and calculated (solid lines) alignment $i = \langle J_x \rangle - \omega J_0 - \omega^3 J_1$ for the GSB's in ^{246}Cm, ^{248}Cf, ^{250}Fm, and ^{252}No ($N = 150$ isotones). The Harris parameters $J_0 = 65\,\hbar^2\text{MeV}^{-1}$ and $J_1 = 200\,\hbar^4\text{MeV}^{-3}$.

orbitals ($j_{15/2}$) decrease slowly. Thus only a small contribution is expected from neutrons to the upbendings for the GSB's in the $N = 150$ isotopes. The band-crossing frequencies for neutrons are about $0.20 \sim 0.25$ MeV, very close to the proton band-crossing frequencies. So neutrons and protons from the high-j orbits compete strongly in rotation alignment as pointed out in Ref. [54].

The contribution of each proton (top row) and neutron (bottom row) major shell to the angular momentum alignment $\langle J_x \rangle$ for the GSB's in the $N = 150$ isotones is shown in Fig. 16. The diagonal $\sum_\mu j_x(\mu)$ and off-diagonal parts $\sum_{\mu<\nu} j_x(\mu\nu)$ in Eq. (5) from the proton $N = 6$ and the neutron $N = 7$ shells are shown by dashed lines. Note that in this figure, the smoothly increasing part of the alignment represented by the Harris formula $(\omega J_0 + \omega^3 J_1)$ is not subtracted (cf. the caption of Fig. 14). It can be seen clearly that the upbendings for the GSB's in ^{246}Cm at $\hbar\omega_c \sim 0.20$ MeV and in ^{248}Cf at $\hbar\omega_c \sim 0.25$ MeV mainly come from the contribution of the proton $N = 6$ shell. Furthermore, the upbending for the GSB in ^{246}Cm is mainly from the off-diagonal part of the proton $N = 6$ shell, while both the diagonal and off-diagonal parts of the proton $N = 6$ shell contribute to the upbending for the GSB in ^{248}Cf. The off-diagonal part of the neutron $N = 7$ shell only contributes a little to the upbending. It is very different from ^{250}Fm and ^{252}No. For these two nuclei, the contribution to the upbending from the off-diagonal parts of the proton $N = 6$ shell and the off-diagonal part of the neutron $N = 7$ shell is nearly the same. This is because that, with the proton number Z increasing, the Fermi surface leaves further and further from the $\pi 7/2^+[633]$ orbital. In this case, the high-j but high-Ω orbital (deformation aligned) $\pi 9/2^+[624]$ becomes close to the Fermi surface.

In order to have a more clear understanding of the upbending mechanism, the contribution of intruder proton orbitals $i_{13/2}$ (top row) and intruder neutron orbitals $j_{15/2}$ (bottom row) to the angular momentum alignments $\langle J_x \rangle$ is presented in Fig. 17. The important diagonal (off-diagonal) part $j_x(\mu)$ [$j_x(\mu\nu)$] in Eq. (5) is denoted by blue solid (red dotted) lines. The orbitals that have no contribution to the upbending (some of these orbitals contribute to the steady increase of the alignment) are denoted by black lines. Near the proton Fermi surfaces of ^{246}Cm and ^{248}Cf, the proton $i_{13/2}$ orbitals are $\pi 5/2^+[642]$ and $\pi 7/2^+[633]$. Other orbitals of $\pi i_{13/2}$ parentage are either fully occupied or fully empty (cf. Fig. 15) and have no contribution to the upbending (only contribute to the steady increase of the alignment). For ^{246}Cm, the PNC calculation shows that after the upbending

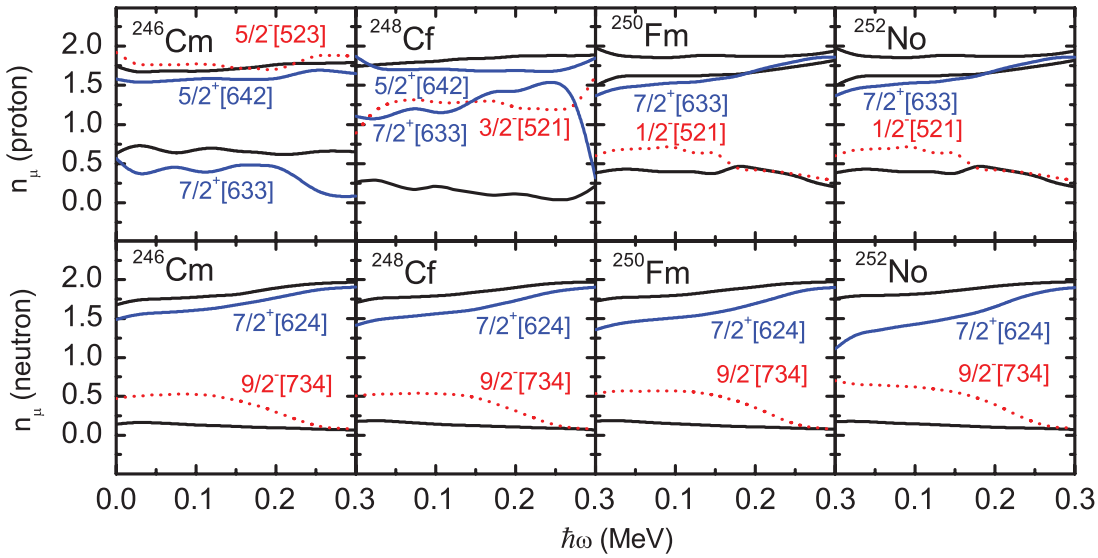

FIG. 15. (Color online) Occupation probability n_μ of each orbital μ (including both $\alpha = \pm 1/2$) near the Fermi surface for the GSB's in ^{246}Cm, ^{248}Cf, ^{250}Fm, and ^{252}No ($N = 150$ isotones). The top and bottom rows are for protons and neutrons, respectively. The positive (negative) parity levels are denoted by blue solid (red dotted) lines. The Nilsson levels far above the Fermi surface ($n_\mu \sim 0$) and far below ($n_\mu \sim 2$) are not shown.

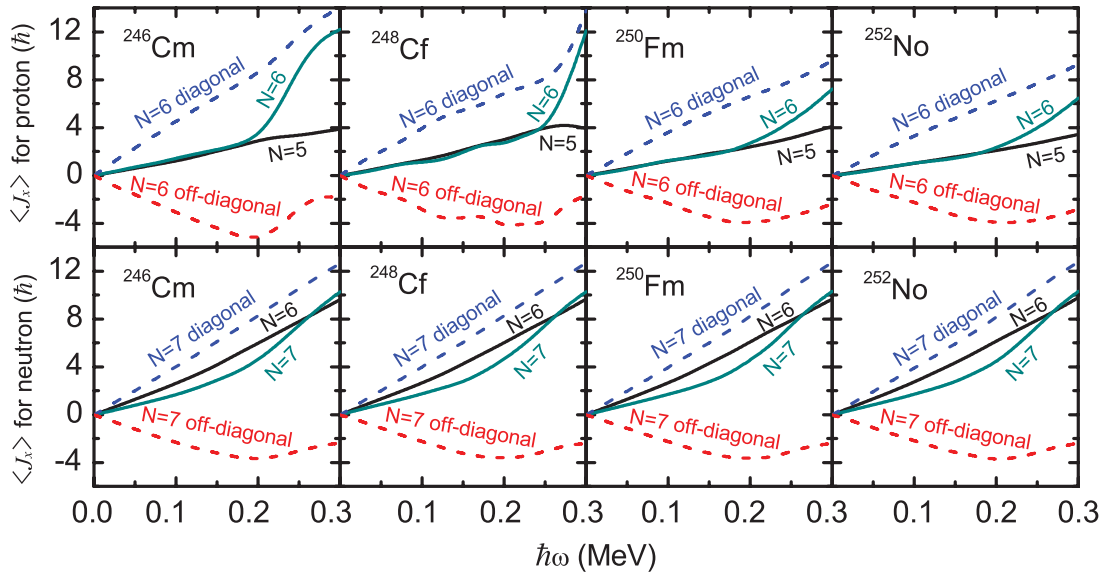

FIG. 16. (Color online) Contribution of each proton (top row) and neutron (bottom) major shell to the angular momentum alignment $\langle J_x \rangle$ for the GSB's in ^{246}Cm, ^{248}Cf, ^{250}Fm, and ^{252}No ($N = 150$ isotones). The diagonal $\sum_\mu j_x(\mu)$ and off-diagonal parts $\sum_{\mu<\nu} j_x(\mu\nu)$ in Eq. (5) from the proton $N = 6$ and neutron $N = 7$ shells are shown by dashed lines.

($\hbar\omega \geqslant 0.20$ MeV) the off-diagonal part $j_x(\pi 5/2^+[642]\pi 7/2^+[633])$ changes a lot. The alignment gain after the upbending mainly comes from this interference term. For ^{248}Cf, the main contribution to the alignment gain after the upbending comes from the diagonal part $j_x(\pi 7/2^+[633])$ and the off-diagonal part $j_x(\pi 5/2^+[642]\pi 7/2^+[633])$. Again this tells us that the upbending in both cases is mainly caused by the $\pi i_{13/2}$ orbitals. As to ^{250}Fm and ^{252}No, only the off-diagonal part $j_x(\pi 7/2^+[633]\pi 9/2^+[624])$ contributes a little to the upbending. The absence of the alignment of $j_{15/2}$ neutrons in nuclei in this mass region can be understood from the contribution of the intruder neutron orbitals ($N = 7$) to $\langle J_x \rangle$. For the nuclei with $N \approx 150$, among the neutron orbitals of $j_{15/2}$ parentage, only the high-Ω (deformation aligned) $\nu 7/2^-[743]$ and $\nu 9/2^-[734]$ are close to the Fermi surface. The diagonal parts of these two orbitals contribute no alignment to the upbending, only the interference term $j_x(\nu 7/2^-[743]\pi 9/2^-[734])$ contributes a little to the alignment. So we can see the strong competition in rotation-alignment between the high-j protons and neutrons in ^{250}Fm and ^{252}No, which is consistent with the result in Ref. [54].

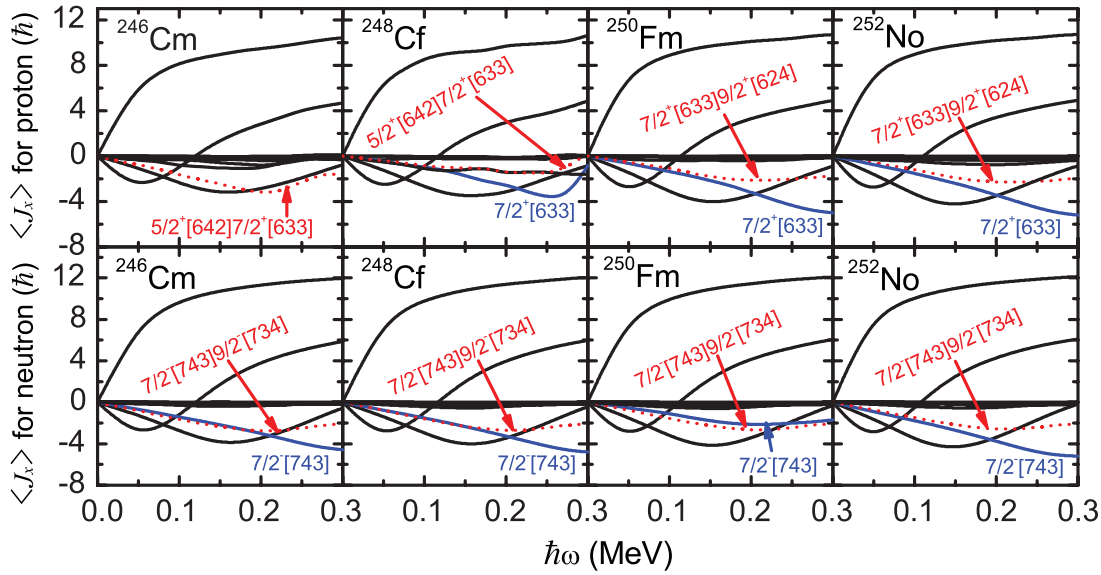

FIG. 17. (Color online) Contribution of each proton orbital in the $N = 6$ major shell (top row) and each neutron orbital in the $N = 7$ major shell (bottom row) to the angular momentum alignments $\langle J_x \rangle$ for the GSB's in ^{246}Cm, ^{248}Cf, ^{250}Fm, and ^{252}No ($N = 150$ isotones). The important diagonal (off-diagonal) part $j_x(\mu)$ [$j_x(\mu\nu)$] in Eq. (5) is denoted by blue solid (red dotted) lines. The orbitals that have no contribution to the upbending (some of these orbitals contribute to the steady increase of the alignment) are denoted by black lines.

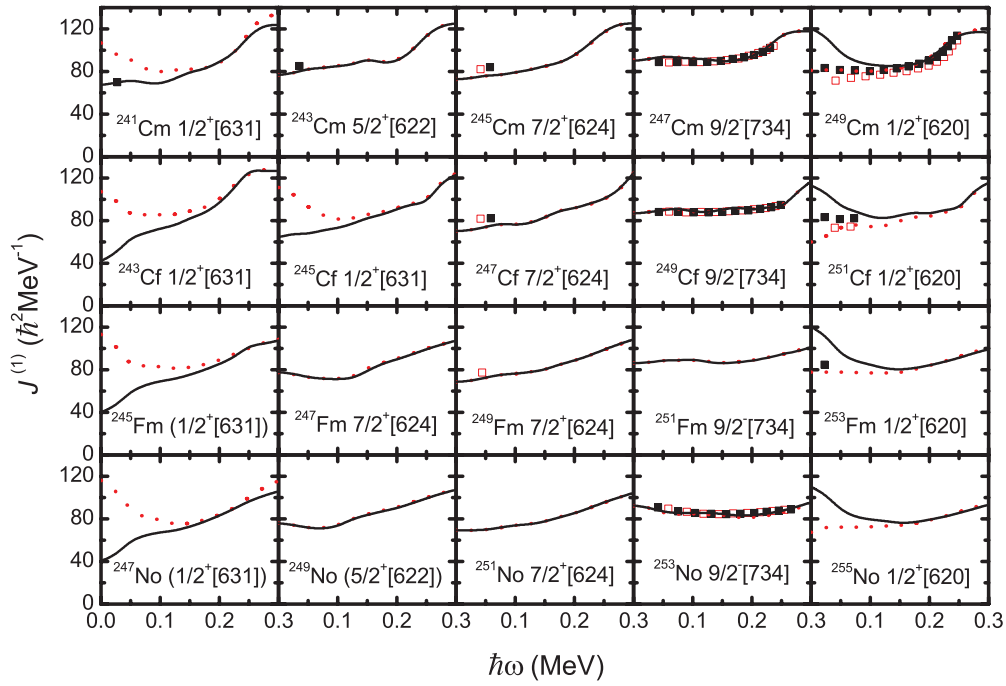

FIG. 18. (Color online) The experimental and calculated MOI's $J^{(1)}$ of the GSB's for odd-N Cm, Cf, Fm, and No isotopes. The data are taken from Ref. [31] and references therein. The most recent data of ^{247,249}Cm and ^{249}Cf are taken from [37]. The experimental MOI's are denoted by full square (signature $\alpha = +1/2$) and open square (signature $\alpha = -1/2$), respectively. The calculated MOI's by the PNC method are denoted by solid lines (signature $\alpha = +1/2$) and dotted lines (signature $\alpha = -1/2$), respectively. The GSB's in the bracket denote the PNC-CSM calculated results which have not been observed. The effective pairing interaction strengths for all these odd-N nuclei are $G_n = 0.25$ MeV, $G_{2n} = 0.015$ MeV, $G_p = 0.40$ MeV, and $G_{2p} = 0.035$ MeV.

D. Odd-A nuclei

It is well known that there exist large fluctuations in the experimental odd-even differences in MOI's $\delta J/J$. If a high-j intruder orbital near the Fermi surface is blocked $\delta J/J$ is quite large (sometime larger than 100%). It is very hard to reproduce the large fluctuations with the conventional BCS method which predicts that $\delta J/J$ is about 15% [111]. One of the advantages of the PNC-CSM is that the Pauli blocking effects are treated exactly. So the odd-even differences in the MOI's $\delta J/J$ can be reproduced quite well and this has been shown for rare-earth nuclei [68]. There are two high-j orbitals involved in the present calculations, namely, $\pi 7/2^+[633]$ ($\pi i_{13/2}$) and $\nu 9/2^-[734]$ ($\nu j_{15/2}$). To show the blocking effects we study the following four nuclei and compare the calculated odd-even differences in MOI's with the data,

$$\frac{\delta J}{J} = \frac{J(^{249}\mathrm{Bk}\,\pi 7/2^+[633]) - J(^{248}\mathrm{Cm\,GSB})}{J(^{248}\mathrm{Cm\,GSB})} \approx 54\%\,(\mathrm{Exp.})\,, \quad 56\%\,(\mathrm{Cal.})\,,$$

$$\frac{\delta J}{J} = \frac{J(^{253}\mathrm{No}\,\nu 9/2^-[734]) - J(^{252}\mathrm{No\,GSB})}{J(^{252}\mathrm{No\,GSB})} \approx 41\%\,(\mathrm{Exp.})\,, \quad 46\%\,(\mathrm{Cal.})\,.$$

It can be seen that the experimentally observed large odd-even difference in MOI's induced by the high-j intruder orbitals can be reproduced quite well.

Figure 18 shows the experimental and calculated MOI's of the GSB's for odd-N Cm, Cf, Fm, and No isotopes ($N = 145$–153). The experimental MOI's are denoted by solid squares (signature $\alpha = +1/2$) and open squares (signature $\alpha = -1/2$), respectively. The calculated MOI's are denoted by solid lines (signature $\alpha = +1/2$) and dotted lines (signature $\alpha = -1/2$), respectively. The experimental MOI's of all these 1-qp bands are well reproduced by the PNC-CSM calculations, which in turn strongly supports the configuration assignments for them. The GSB's in the bracket denote the PNC-CSM calculated results which have not been observed. We should note that the pairing strengths used in Ref. [57] are a little different with what we used now. This is because the pairing strengths are considered as an average for all of these odd-N nuclei.

In the $N = 145$ isotones, our calculations predict a significant signature splitting at the low rotational frequency ($\hbar\omega < 0.20$ MeV) for the $\nu 1/2^+[631]$ orbital. In the $N = 153$ isotones, the signature splitting of the $\nu 1/2^+[620]$ orbital is well reproduced by our calculation, too. It is understandable from the behavior of the cranked Nilsson orbital $\nu 1/2^+[631]$ and $\nu 1/2^+[620]$ in Fig. 3. In Ref. [57], we have already analyzed the upbending mechanism for the high-spin rotational GSB's of ^{247,249}Cm and ^{249}Cf observed in Ref. [37].

Figure 19 shows the results of excited 1-qp bands observed in the odd-A Cm, Cf, Fm, and No isotopes. They are all well reproduced by the PNC-CSM calculation. It is interesting to noted that, in an earlier experiment for ^{253}No, a rotational band has been established and the configuration was assigned as $\nu 7/2^+[624]$. In a latter experiment, a similar rotational band has been observed [39], but the configuration was assigned

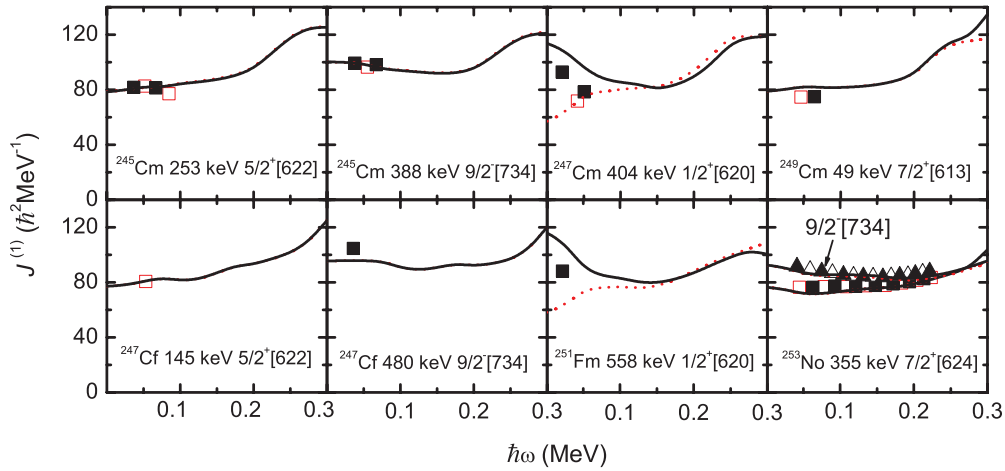

FIG. 19. (Color online) The same as Fig. 18, but for the excited 1-qp bands in odd-N Cm, Cf, and No isotopes. The data of ^{253}No are taken from [38]. Our calculated results according to two configuration assignments for this band, $\nu 9/2^-[734]$ and $\nu 7/2^+[624]$, are shown by squares and triangles, respectively.

as $\nu 9/2^-[734]$. It can be seen that, the experimental MOI's extracted from [38] using these two configurations can be reproduced by the PNC calculations. So from our calculation, it can not be distinguished which configuration assignment is correct.

Figure 20 is the experimental and calculated GSB's of the odd-Z nuclei, including Bk, Es, and Md isotopes (N = 146–154). The data for these odd-Z nuclei are very rare. Most of the data are well reproduced, except the $\pi 7/2^+[633]$ band in ^{253}Es. The MOI of this band seems extremely large, $J^{(1)}$ is larger than 120 $\hbar^2$MeV^{-1}. Our calculations show that the $\pi 7/2^+[633]$ has a small signature splitting at the higher rotational frequency ($\hbar\omega > 0.10$ MeV).

Figure 21 shows the results of excited 1-qp bands observed in the odd-Z Bk, Es, and Md isotopes. In some nuclei there exists an upbending around $\hbar\omega \approx 0.25$ MeV in the $\pi 7/2^+[633]$ (signature $\alpha = 1/2$) band according to the PNC calculations (i.e., the Bk isotopes). We show the occupation probabilities n_μ of each orbital μ near the Fermi surface of the $\pi 7/2^+[633]$ ($\alpha = 1/2$) band in ^{249}Bk. The top and bottom rows are for protons and neutrons, respectively. The positive (negative) parity levels are denoted by blue solid (red dotted) lines. It is clearly seen that the occupation probabilities of $\pi 5/2^+[642]$ and $\pi 7/2^+[633]$ orbitals drop sharply at $\hbar\omega \approx 0.25$ MeV, while n_μ of $\pi 3/2^-[521]$ increases sharply. The occupation probabilities of the neutron orbitals change slowly with increasing $\hbar\omega$, indicating little contribution to the

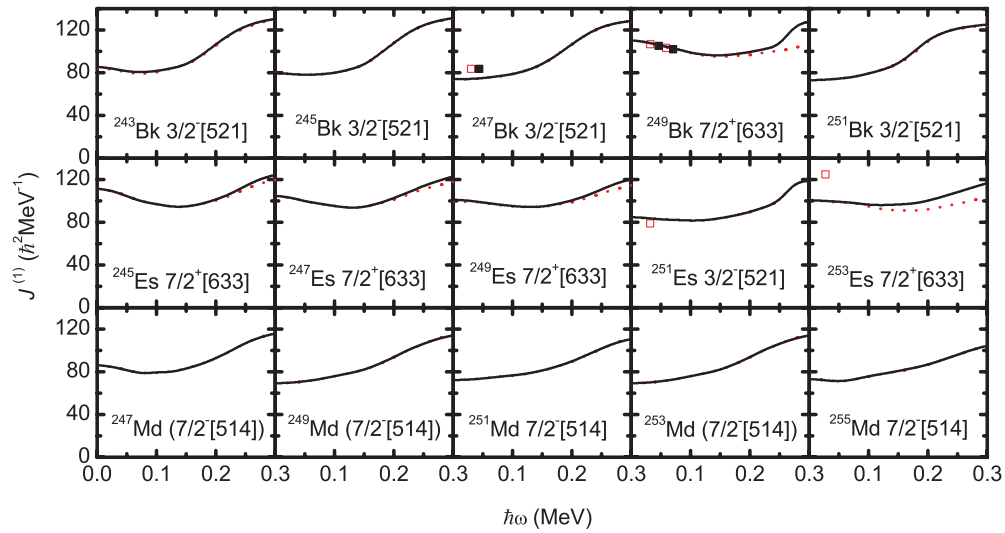

FIG. 20. (Color online) The experimental and calculated MOI's $J^{(1)}$ of the GSB's for odd-Z Bk, Es, and Md isotopes. The data are taken from Ref. [31] and references therein. The experimental MOI's are denoted by full square (signature $\alpha = +1/2$) and open square (signature $\alpha = -1/2$), respectively. The calculated MOI's by the PNC method are denoted by solid lines (signature $\alpha = +1/2$) and dotted lines (signature $\alpha = -1/2$), respectively. The states in the bracket denote that the GSB's have not been observed. The effective pairing interaction strengths for all these odd-Z nuclei are, $G_n = 0.30$ MeV, $G_{2n} = 0.02$ MeV, $G_p = 0.25$ MeV, and $G_{2p} = 0.01$ MeV.

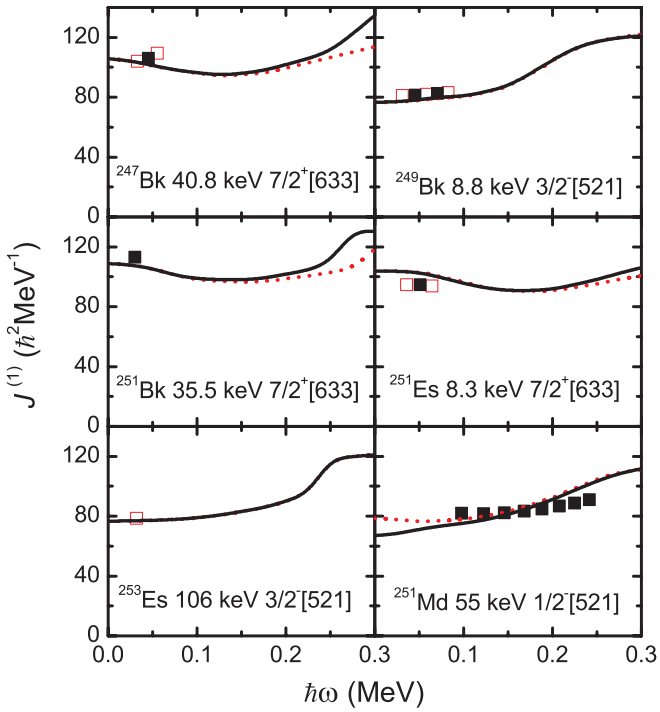

FIG. 21. (Color online) The same as Fig. 20, but for the excited 1-qp bands in odd-Z Bk, Es, and Md isotopes.

upbending. Figure 23 shows the contribution of each proton (top row) and neutron (bottom row) major shell to the angular momentum alignment $\langle J_x \rangle$ for the $\pi 7/2^+[633]$ ($\alpha = 1/2$) band in ^{249}Bk. The diagonal $\sum_\mu j_x(\mu)$ and off-diagonal part $\sum_{\mu<\nu} j_x(\mu\nu)$ in Eq. (5) from the proton $N = 6$ and neutron $N = 7$ shells are shown by dashed lines. It can be seen from Fig. 23 that, both the diagonal and off-diagonal part from proton $N = 6$ shell contribute to the upbending. The PNC calculation shows that the upbending comes

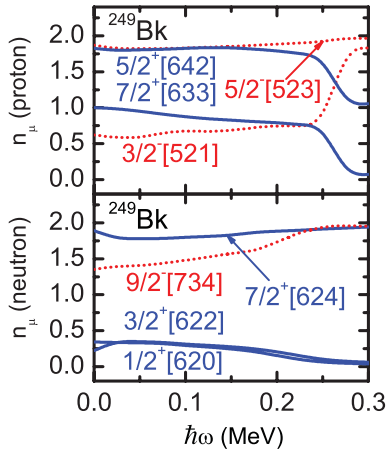

FIG. 22. (Color online) Occupation probability n_μ of each orbital μ near the Fermi surface of the $\pi 7/2^+[633]$ ($\alpha = 1/2$) band in ^{249}Bk. The top and bottom rows are for protons and neutrons respectively. The positive (negative) parity levels are denoted by blue solid (red dotted) lines. The Nilsson levels far above the Fermi surface ($n_\mu \sim 0$) and far below ($n_\mu \sim 2$) are not shown.

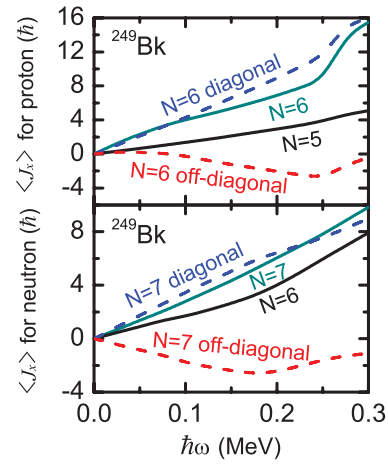

FIG. 23. (Color online) Contribution of each proton (top row) and neutron (bottom row) major shell to the angular momentum alignment $\langle J_x \rangle$ for the $\pi 7/2^+[633]$ ($\alpha = 1/2$) band in ^{249}Bk. The diagonal part $\sum_\mu j_x(\mu)$ and off-diagonal part $\sum_{\mu<\nu} j_x(\mu\nu)$ in Eq. (5) from the proton $N = 6$ and neutron $N = 7$ shells are shown by dashed lines.

from the diagonal parts $j_x(\pi 5/2^+[642])$ and $j_x(\pi 7/2^+[633])$, and the off-diagonal parts $j_x(\pi 5/2^+[642]\pi 7/2^+[633])$ and $j_x(\pi 7/2^+[633]\pi 9/2^+[624])$.

E. Odd-odd nuclei

When an unpaired proton and an unpaired neutron in a deformed odd-odd nucleus are coupled, the projections of their total angular momentum on the nuclear symmetry axis, Ω_p and Ω_n, can produce two states with $K_> = |\Omega_p + \Omega_n|$ and $K_< = |\Omega_p - \Omega_n|$. They follow the Gallagher-Moszkowski (GM) coupling rules [113]:

$$K_> = |\Omega_p + \Omega_n|, \text{ if } \Omega_p = \Lambda_p \pm \tfrac{1}{2} \text{ and } \Omega_n = \Lambda_n \pm \tfrac{1}{2},$$
$$K_< = |\Omega_p - \Omega_n|, \text{ if } \Omega_p = \Lambda_p \pm \tfrac{1}{2} \text{ and } \Omega_n = \Lambda_n \mp \tfrac{1}{2}.$$

The rotational bands in odd-odd nuclei in the transfermium region are very rare. The most recent experiment is for ^{250}Bk [112]. In [112], the energy splittings between parallel and antiparallel coupled neutron and proton states were measured for six pairs of states. Because the residual proton-neutron interaction is not included in our calculations, the energies of the 2-qp bands in odd-odd nuclei are the sum of the quasiproton and the quasineutron, that is to say, there is no energy splitting between states with parallel and antiparallel coupling.

Figure 24 shows the experimental and calculated MOI's of the 2-qp bands in ^{250}Bk. The energy of neutron orbital $\nu 1/2^-[750]$ is too high in our calculation, so we do not take into account the $K^\pi = 3^-, 4^-(\pi 7/2^+[633] \otimes \nu 1/2^-[750])$ bands observed in Ref. [112]. The up (down) triangles denote the experimental value of $K_>$ ($K_<$) bands. The filled (open) triangles denote the signature $\alpha = 0$ (1) bands. The solid (dotted) lines denote the calculated results with signature $\alpha = 0$ (1) bands. Most of the data are reproduced quite well. The calculated MOI's are a little smaller in the $K^\pi = 2^+, 5^+$ bands than the experimental values, while much larger in the $K^\pi = 1^-$ band.

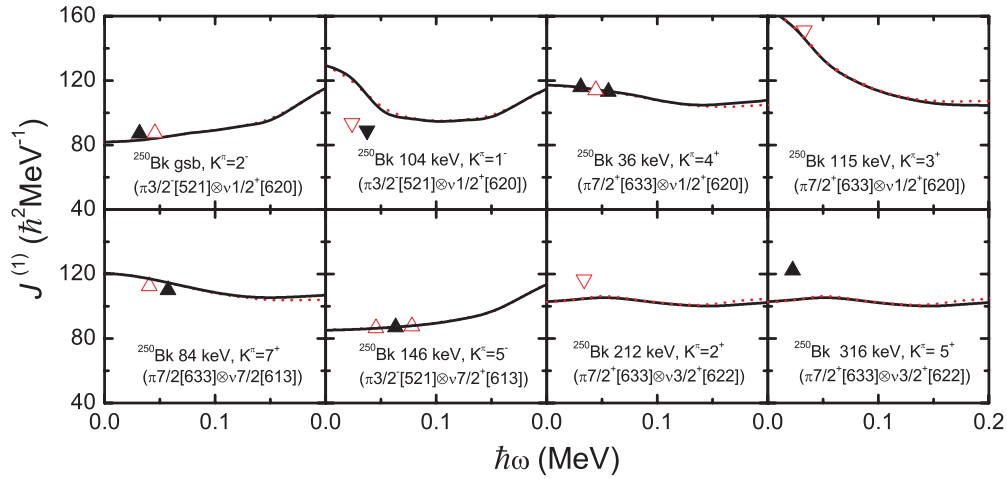

FIG. 24. (Color online) The experimental and calculated MOI's of the 2-qp bands in ^{250}Bk. The data are taken from [90,112]. The up (down) triangles denote the experimental value of $K_>$ ($K_<$) bands. The filled (open) triangles denote the signature $\alpha = 0$ (1) bands. The solid (dotted) lines denote the calculated results with signature $\alpha = 0$ (1) bands. The effective pairing interaction strengths for both protons and neutrons are $G_n = 0.25$ MeV, $G_{2n} = 0.015$ MeV, $G_p = 0.25$ MeV, and $G_{2p} = 0.010$ MeV.

The MOI's of a $K_>$ and the corresponding $K_<$ bands are usually the same. But the MOI's of the $K^\pi = 3^+$ band are much larger than those of the $K^\pi = 4^+$ band. This is because for the $K^\pi = 3^+$ band, the neutron component is $\nu 1/2^+[620](\alpha = +1/2)$, whereas for the $K^\pi = 4^+$ band, the neutron component is $\nu 1/2^+[620](\alpha = -1/2)$ and the signature splitting of $\nu 1/2^+[620]$ is very large. The calculated results are very close to the data. Similarly, our calculation predicts that this signature splitting results in big differences between the MOI's of the $K^\pi = 1^-$ and 2^- bands. However, this is not the case in the experiment. It is well known that when one of the nucleons is in an $\Omega = 1/2$ orbital, the GM doublet has $\Delta K = 1$, accordingly the two bands are expected to be Coriolis admixed. This effect can be very significant in the $K_<$ band, which has been identified in the odd-odd rare-earth nuclei [114,115]. The similar MOI's in the $K^\pi = 1^-$ and 2^- bands may be from this mixing and need to be further explored both experimentally and theoretically.

V. SUMMARY

In summary, the rotational bands in the $A \approx 250$ mass region are investigated using a cranked shell model (CSM) with the pairing correlations treated by a particle-number conserving (PNC) method. In the PNC method for the pairing correlations, the blocking effects are taken into account exactly. By fitting the experimental single-particle spectra in these nuclei, a new set of Nilsson parameters (κ and μ) and deformation parameters (ε_2 and ε_4) are proposed. The band-head energies of 1-qp states with energies less than 0.8 MeV are reproduced satisfactorily. The experimentally observed ω variations of MOI's for the even-even, odd-A, and odd-odd nuclei are reproduced very well by the PNC-CSM calculations. By analyzing the ω dependence of the occupation probability of each cranked Nilsson orbital near the Fermi surface and the contributions of valence orbitals in each major shell to the angular momentum alignment, the upbending mechanism in this region is understood clearly. For Cm and Cf isotopes, the upbending in the GSB's is mainly caused by the intruder proton ($N = 6$) $\pi i_{13/2}$ orbitals. For Fm and No isotopes, neutrons and protons from the high-j orbits compete strongly in rotation alignment. The 2-qp states in the odd-odd nuclei ^{250}Bk are analyzed in detail.

ACKNOWLEDGMENTS

Helpful discussions with G. Adamian, N. Antonenko, B. A. Brown, N. V. Giai, R. V. Jolos, J. Meng, P. Ring, F. Sakata, Y. Sun, and D. Vretenar are gratefully acknowledged. This work has been supported by NSFC (Grant Nos. 10705014, 10875157, 10975100, 10979066, 11175252, and 11120101005), MOST (973 Project 2007CB815000), CAS (Grant Nos. KJCX2-EW-N01 and KJCX2-YW-N32), and FRF for NUAA (Grant No. NS2010157). The computation of this work was supported by Supercomputing Center, CNIC of CAS.

[1] W. D. Myers and W. J. Swiatecki, Nucl. Phys. **81**, 1 (1966).
[2] A. Sobiczewski, F. Gareev, and B. Kalinkin, Phys. Lett. **22**, 500 (1966).
[3] H. Meldner, Arkiv Fysik **36**, 593 (1967); Proceedings of the Lysekil Symposium: Nuclides far off the Stability Line, Aug. 21–27, 1966, Sweden.
[4] S. G. Nilsson, J. R. Nix, A. Sobiczewski, Z. Szymanski, S. Wycech, C. Gustafson, and P. Möller, Nucl. Phys. A **115**, 545 (1968); S. G. Nilsson, S. G. Thompson, and C. F. Tsang, Phys. Lett. B **28**, 458 (1969); S. G. Nilsson, C. F. Tsang, A. Sobiczewski, Z. Szymanski, S. Wycech, C. Gustafson, I.-L. Lamm, P. Möller, and B. Nilsson, Nucl. Phys. A **131**, 1 (1969).

[5] U. Mosel and W. Greiner, Z. Phys. A **222**, 261 (1969); J. Grumann, U. Mosel, B. Fink, and W. Greiner, *ibid.* **228**, 371 (1969).

[6] S. Hofmann and G. Münzenberg, Rev. Mod. Phys. **72**, 733 (2000).

[7] K. Morita *et al.*, J. Phys. Soc. Jpn. **73**, 2593 (2004).

[8] Y. Oganessian, J. Phys. G: Nucl. Phys. **34**, R165 (2007); Y. T. Oganessian *et al.*, Phys. Rev. Lett. **104**, 142502 (2010).

[9] A. Sobiczewski and K. Pomorski, Prog. Part. Nucl. Phys. **58**, 292 (2007).

[10] S. Cwiok and A. Sobiczewski, Z. Phys. A **342**, 203 (1992).

[11] P. Möller, J. R. Nix, W. D. Myers, and W. J. Swiatecki, At. Data Nucl. Data Tables **59**, 185 (1995).

[12] A. Mamdouh, J. M. Pearson, M. Rayet, and F. Tondeur, Nucl. Phys. A **679**, 337 (2001).

[13] K. Rutz, M. Bender, T. Burvenich, T. Schilling, P.-G. Reinhard, J. A. Maruhn, and W. Greiner, Phys. Rev. C **56**, 238 (1997); M. Bender, K. Rutz, P.-G. Reinhard, J. A. Maruhn, and W. Greiner, *ibid.* **60**, 034304 (1999); A. T. Kruppa, M. Bender, W. Nazarewicz, P.-G. Reinhard, T. Vertse, and S. Cwiok, *ibid.* **61**, 034313 (2000).

[14] G. A. Lalazissis, M. M. Sharma, P. Ring, and Y. K. Gambhir, Nucl. Phys. A **608**, 202 (1996).

[15] W. Zhang, J. Meng, S. Zhang, L. Geng, and H. Toki, Nucl. Phys. A **753**, 106 (2005).

[16] J. Meng, H. Toki, S. G. Zhou, S. Q. Zhang, W. H. Long, and L. S. Geng, Prog. Part. Nucl. Phys. **57**, 470 (2006).

[17] G. G. Adamian, N. V. Antonenko, W. Scheid, and V. V. Volkov, Nucl. Phys. A **633**, 409 (1998); Phys. Rev. C **69**, 011601 (2004); A. Zubov, G. Adamian, and N. Antonenko, Phys. Part. Nucl. **40**, 847 (2009).

[18] W. Li, N. Wang, J. F. Li, H. Xu, W. Zuo, E. Zhao, J. Q. Li, and W. Scheid, Europhys. Lett. **64**, 750 (2003).

[19] E. G. Zhao, N. Wang, Z. Q. Feng, J. Q. Li, S. G. Zhou, and W. Scheid, Int. J. Mod. Phys. E **17**, 1937 (2008); Proceedings of International Workshop on Nuclear Dynamics in Heavy-ion Reactions and Neutron Stars, Beijing, July 9–14, 2007.

[20] J.-Q. Li, Z.-Q. Feng, Z.-G. Gan, X.-H. Zhou, H.-F. Zhang, and W. Scheid, *The 10th International Conference on Nucleus-Nucleus Collisions (NN2009)* [Nucl. Phys. A **834**, 353c (2010)].

[21] Z.-Q. Feng, G.-M. Jin, and J.-Q. Li, Nucl. Phys. Rev. **28**, 1 (2011).

[22] W. J. Swiatecki, K. Siwek-Wilczynska, and J. Wilczynski, Phys. Rev. C **71**, 014602 (2005).

[23] Z. H. Liu and J.-D. Bao, Phys. Rev. C **76**, 034604 (2007); **80**, 034601 (2009); Sci. China Ser. G-Phys. Mech. Astron. **52**, 1482 (2009).

[24] V. I. Zagrebaev, Phys. Rev. C **64**, 034606 (2001); V. Zagrebaev and W. Greiner, J. Phys. G: Nucl. Part. Phys. **31**, 825 (2005); Phys. Rev. C **78**, 034610 (2008).

[25] B.-A. Bian, F.-S. Zhang, and H.-Y. Zhou, Nucl. Phys. A **829**, 1 (2009); S. S. Du, B. A. Bian, M. Liu, Z. Q. Feng, and F. S. Zhang, Sci. China Ser. G-Phys. Mech. Astron. **52**, 1489 (2009).

[26] Y. Abe, C. Shen, G. Kosenko, and D. Boilley, Phys. At. Nucl. **66**, 1057 (2003); C. Shen, G. Kosenko, and Y. Abe, Phys. Rev. C **66**, 061602(R) (2002); C. W. Shen, Y. Abe, Q. F. Li, and D. Boilley, Sci. China Ser. G-Phys. Mech. Astron. **52**, 1458 (2009).

[27] G. G. Adamian, N. V. Antonenko, S. P. Ivanova, and W. Scheid, Phys. Rev. C **62**, 064303 (2000); G. G. Adamian, N. V. Antonenko, and V. V. Sargsyan, *ibid.* **79**, 054608 (2009).

[28] C.-J. Xia, B.-X. Sun, E.-G. Zhao, and S.-G. Zhou, Sci. China-Phys. Mech. Astron. **54** (Suppl. 1), 109 (2011).

[29] M. Leino and F. P. Hessberger, Annu. Rev. Nucl. Part. Sci. **54**, 175 (2004).

[30] D. Ackermann, Acta Phys. Pol. B **42**, 577 (2011).

[31] R.-D. Herzberg, J. Phys. G: Nucl. Phys. **30**, R123 (2004); R.-D. Herzberg and P. Greenlees, Prog. Part. Nucl. Phys. **61**, 674 (2008).

[32] P. T. Greenlees, Acta Phys. Pol. B **42**, 587 (2011).

[33] P. Reiter *et al.*, Phys. Rev. Lett. **82**, 509 (1999).

[34] J. E. Bastin *et al.*, Phys. Rev. C **73**, 024308 (2006).

[35] R.-D. Herzberg *et al.*, Phys. Rev. C **65**, 014303 (2001).

[36] R. Takahashi *et al.*, Phys. Rev. C **81**, 057303 (2010).

[37] S. K. Tandel *et al.*, Phys. Rev. C **82**, 041301(R) (2010).

[38] P. Reiter *et al.*, Phys. Rev. Lett. **95**, 032501 (2005).

[39] R. Herzberg *et al.*, Eur. Phys. J. A **42**, 333 (2009).

[40] A. Chatillon *et al.*, Phys. Rev. Lett. **98**, 132503 (2007).

[41] S. Ketelhut *et al.*, Phys. Rev. Lett. **102**, 212501 (2009).

[42] A. V. Afanasjev, T. L. Khoo, S. Frauendorf, G. A. Lalazissis, and I. Ahmad, Phys. Rev. C **67**, 024309 (2003).

[43] M. Bender, P. Bonche, T. Duguet, and P. H. Heenen, Nucl. Phys. A **723**, 354 (2003).

[44] J.-P. Delaroche, M. Girod, H. Goutte, and J. Libert, Nucl. Phys. A **771**, 103 (2006).

[45] G. G. Adamian, N. V. Antonenko, L. A. Malov, B. N. Lu, S. G. Zhou, and W. Scheid, Phys. Part. Nucl. **41**, 1101 (2010); G. G. Adamian, N. V. Antonenko, S. N. Kuklin, B. N. Lu, L. A. Malov, and S. G. Zhou, Phys. Rev. C **84**, 024324 (2011).

[46] S. Cwiok, S. Hofmann, and W. Nazarewicz, Nucl. Phys. A **573**, 356 (1994).

[47] I. Muntian, Z. Patyk, and A. Sobiczewski, Phys. Rev. C **60**, 041302(R) (1999).

[48] A. Sobiczewski, I. Muntian, and Z. Patyk, Phys. Rev. C **63**, 034306 (2001).

[49] A. Parkhomenko and A. Sobiczewski, Acta Phys. Pol. B **35**, 2447 (2004).

[50] A. Parkhomenko and A. Sobiczewski, Acta Phys. Pol. B **36**, 3115 (2005).

[51] G. G. Adamian, N. V. Antonenko, and W. Scheid, Phys. Rev. C **81**, 024320 (2010); G. G. Adamian, N. V. Antonenko, S. N. Kuklin, and W. Scheid, *ibid.* **82**, 054304 (2010).

[52] Y. Sun, G.-L. Long, F. Al-Khudair, and J. A. Sheikh, Phys. Rev. C **77**, 044307 (2008).

[53] Y.-S. Chen, Y. Sun, and Z.-C. Gao, Phys. Rev. C **77**, 061305(R) (2008).

[54] F. Al-Khudair, G.-L. Long, and Y. Sun, Phys. Rev. C **79**, 034320 (2009).

[55] F. R. Xu, E. G. Zhao, R. Wyss, and P. M. Walker, Phys. Rev. Lett. **92**, 252501 (2004).

[56] X.-T. He, Z.-Z. Ren, S.-X. Liu, and E.-G. Zhao, Nucl. Phys. A **817**, 45 (2009).

[57] Z.-H. Zhang, J.-Y. Zeng, E.-G. Zhao, and S.-G. Zhou, Phys. Rev. C **83**, 011304(R) (2011).

[58] R. V. Jolos, L. A. Malov, N. Y. Shirikova, and A. V. Sushkov, J. Phys. G: Nucl. Part. Phys. **38**, 115103 (2011).

[59] K. Zhuang, Z.-B. Li, and Y.-X. Liu, Commun. Theor. Phys. **57**, 271 (2012).

[60] J.-W. Cui, X.-R. Zhou, F.-Q. Chen, Y. Sun, C.-L. Wu, and H. Zhao, "Study on the band structure of the actinide-region nuclei by heavy shell model" (in preparation).

[61] J. Y. Zeng and T. S. Cheng, Nucl. Phys. A **405**, 1 (1983).

[62] J. Y. Zeng, T. H. Jin, and Z. J. Zhao, Phys. Rev. C **50**, 1388 (1994).
[63] C. S. Wu and J. Y. Zeng, Phys. Rev. C **39**, 666 (1989).
[64] J. Meng, J.-y. Guo, L. Liu, and S.-q. Zhang, Frontiers Phys. China **1**, 38 (2006).
[65] N. Pillet, P. Quentin, and J. Libert, Nucl. Phys. A **697**, 141 (2002).
[66] X. B. Xin, S. X. Liu, Y. A. Lei, and J. Y. Zeng, Phys. Rev. C **62**, 067303 (2000).
[67] H. Molique and J. Dudek, Phys. Rev. C **56**, 1795 (1997).
[68] J. Y. Zeng, Y. A. Lei, T. H. Jin, and Z. J. Zhao, Phys. Rev. C **50**, 746 (1994).
[69] C. S. Wu and J. Y. Zeng, Phys. Rev. C **41**, 1822 (1990).
[70] Z. H. Zhang, X. Wu, Y. A. Lei, and J. Y. Zeng, Nucl. Phys. A **816**, 19 (2009).
[71] Z. H. Zhang, Y. A. Lei, and J. Y. Zeng, Phys. Rev. C **80**, 034313 (2009).
[72] S. X. Liu, J. Y. Zeng, and L. Yu, Nucl. Phys. A **735**, 77 (2004).
[73] B. R. Chen, T. Li, and S. X. Liu, Sci. China Ser. G-Phys. Mech. Astron. **52**, 1542 (2009).
[74] X. He, S. Yu, J. Zeng, and E. Zhao, Nucl. Phys. A **760**, 263 (2005).
[75] S. X. Liu and J. Y. Zeng, Phys. Rev. C **66**, 067301 (2002).
[76] J. Y. Zeng, S. X. Liu, Y. A. Lei, and L. Yu, Phys. Rev. C **63**, 024305 (2001).
[77] S. X. Liu, J. Y. Zeng, and E. G. Zhao, Phys. Rev. C **66**, 024320 (2002).
[78] X. Wu, Z. H. Zhang, J. Y. Zeng, and Y. A. Lei, Phys. Rev. C **83**, 034323 (2011).
[79] T. Bengtsson and I. Ragnarsson, Nucl. Phys. A **436**, 14 (1985).
[80] T. Seo, Z. Phys. A **324**, 43 (1986).
[81] J.-y. Zhang, Y. Sun, M. Guidry, L. L. Riedinger, and G. A. Lalazissis, Phys. Rev. C **58**, R2663 (1998).
[82] Y. Sun, J.-y. Zhang, M. Guidry, J. Meng, and S. Im, Phys. Rev. C **62**, 021601(R) (2000).
[83] T. M. Shneidman, G. G. Adamian, N. V. Antonenko, and R. V. Jolos, Phys. Rev. C **74**, 034316 (2006).
[84] B.-N. Lu, E.-G. Zhao, and S.-G. Zhou, Phys. Rev. C **85**, 011301(R) (2012).
[85] R. R. Chasman, I. Ahmad, A. M. Friedman, and J. R. Erskine, Rev. Mod. Phys. **49**, 833 (1977); **50**, 173 (1978).
[86] M. Martin, Nucl. Data Sheets **106**, 89 (2005).
[87] F. P. Hessberger, S. Hofmann, D. Ackermann, P. Cagarda, R. D. Herzberg, I. Kojouharov, P. Kuusiniemi, M. Leino, and R. Mann, Eur. Phys. J. A **22**, 417 (2004).
[88] T. H. Braid, R. R. Chasman, J. R. Erskine, and A. M. Friedman, Phys. Rev. C **4**, 247 (1971).
[89] F. Hessberger *et al.*, Eur. Phys. J. A **30**, 561 (2006).
[90] R. Firestone, C. M. Baglin, and S. Y. Frank Chu, *Table of Isotopes: 1999 Update with CD-ROM* (Wiley, New York, 1999).
[91] Y. A. Akovali, Nucl. Data Sheets **102**, 515 (2004).
[92] F. P. Hessberger, Eur. Phys. J. D **45**, 33 (2007).
[93] M. Asai *et al.*, Phys. Rev. C **83**, 014315 (2011).
[94] I. Ahmad, R. R. Chasman, J. P. Greene, F. G. Kondev, E. F. Moore, E. Browne, C. E. Porter, and L. K. Felker, Phys. Rev. C **68**, 044306 (2003).
[95] H. Makii *et al.*, Phys. Rev. C **76**, 061301(R) (2007).
[96] A. Lopez-Martens *et al.*, Eur. Phys. J. A **32**, 245 (2007).
[97] S. W. Yates, R. R. Chasman, A. M. Friedman, I. Ahmad, and K. Katori, Phys. Rev. C **12**, 442 (1975).
[98] T. Ishii *et al.*, Phys. Rev. C **78**, 054309 (2008).
[99] I. Ahmad, J. P. Greene, E. F. Moore, F. G. Kondev, R. R. Chasman, C. E. Porter, and L. K. Felker, Phys. Rev. C **72**, 054308 (2005).
[100] M. Asai *et al.*, Phys. Rev. Lett. **95**, 102502 (2005).
[101] F. Hessberger *et al.*, Eur. Phys. J. A **29**, 165 (2006).
[102] H. Yuichi *et al.*, Nucl. Phys. A **500**, 90 (1989).
[103] I. Ahmad, S. W. Yates, R. K. Sjoblom, and A. M. Friedman, Phys. Rev. C **20**, 290 (1979).
[104] I. Ahmad *et al.*, Phys. Rev. C **71**, 054305 (2005).
[105] J. Tuli, S. Singh, and A. K. Jain, Nucl. Data Sheets **107**, 1347 (2006).
[106] I. Ahmad, R. K. Sjoblom, A. M. Friedman, and S. W. Yates, Phys. Rev. C **17**, 2163 (1978).
[107] F. Hessberger *et al.*, Eur. Phys. J. A **26**, 233 (2005).
[108] I. Ahmad, R. R. Chasman, and P. R. Fields, Phys. Rev. C **61**, 044301 (2000).
[109] A. Chatillon *et al.*, Eur. Phys. J. A **30**, 397 (2006).
[110] F. S. Stephens, Rev. Mod. Phys. **47**, 43 (1975).
[111] A. Bohr and B. R. Mottelson, *Nuclear Structure*, 1st ed., Vol. II (Benjamin, New York, 1975).
[112] I. Ahmad, F. G. Kondev, Z. M. Koenig, W. C. McHarris, and S. W. Yates, Phys. Rev. C **77**, 054302 (2008).
[113] C. J. Gallagher and S. A. Moszkowski, Phys. Rev. **111**, 1282 (1958).
[114] R. O'neil and D. Burke, Nucl. Phys. A **195**, 207 (1972).
[115] A. K. Jain, R. K. Sheline, D. M. Headly, P. C. Sood, D. G. Burke, I. Hrivnacova, J. Kvasil, D. Nosek, and R. W. Hoff, Rev. Mod. Phys. **70**, 843 (1998).